

# The Remarkable Reactivity of High Oxidation State Ruthenium and Osmium Polypyridyl Complexes

Thomas J. Meyer<sup>\*,†,‡</sup> and My Hang V. Huynh<sup>†</sup>

Strategic Research, MS A127, Los Alamos National Laboratory, P.O. Box 1663, Los Alamos, New Mexico 87545, and Department of Chemistry, The University of North Carolina at Chapel Hill, Chapel Hill, North Carolina 27599-3290

Received December 30, 2002

There is a remarkable redox chemistry of higher oxidation state M(IV)–M(VI) polypyridyl complexes of Ru and Os. They are accessible by proton loss and formation of oxo or nitrido ligands, examples being *cis*-[Ru<sup>IV</sup>(bpy)<sub>2</sub>(py)(O)]<sup>2+</sup> (Ru<sup>IV</sup>=O<sup>2+</sup>, bpy = 2,2'-bipyridine, and py = pyridine) and *trans*-[Os<sup>VI</sup>(tpy)(Cl)<sub>2</sub>(N)]<sup>+</sup> (tpy = 2,2':6',2''-terpyridine). Metal–oxo or metal–nitrido multiple bonding stabilizes the higher oxidation states and greatly influences reactivity. O-atom transfer, hydride transfer, epoxidation, C–H insertion, and proton-coupled electron-transfer mechanisms have been identified in the oxidation of organics by Ru<sup>IV</sup>=O<sup>2+</sup>. The Ru–O multiple bond inhibits electron transfer and promotes complex mechanisms. Both O atoms can be used for O-atom transfer by *trans*-[Ru<sup>VI</sup>(tpy)(O)<sub>2</sub>(S)]<sup>2+</sup> (S = CH<sub>3</sub>CN or H<sub>2</sub>O). Four-electron, four-proton oxidation of *cis,cis*-[(bpy)<sub>2</sub>(H<sub>2</sub>O)Ru<sup>III</sup>–O–Ru<sup>III</sup>(H<sub>2</sub>O)(bpy)<sub>2</sub>]<sup>4+</sup> occurs to give *cis,cis*-[(bpy)<sub>2</sub>(O)Ru<sup>V</sup>–O–Ru<sup>V</sup>(O)(bpy)<sub>2</sub>]<sup>4+</sup> which rapidly evolves O<sub>2</sub>. Oxidation of NH<sub>3</sub> in *trans*-[Os<sup>II</sup>(tpy)(Cl)<sub>2</sub>(NH<sub>3</sub>)] gives *trans*-[Os<sup>VI</sup>(tpy)(Cl)<sub>2</sub>(N)]<sup>+</sup> through a series of one-electron intermediates. It and related nitrido complexes undergo formal N<sup>−</sup> transfer analogous to O-atom transfer by Ru<sup>IV</sup>=O<sup>2+</sup>. With secondary amines, the products are the hydrazido complexes, *cis*- and *trans*-[Os<sup>V</sup>(L<sub>3</sub>)(Cl)<sub>2</sub>(NNR<sub>2</sub>)]<sup>+</sup> (L<sub>3</sub> = tpy or tpm and NR<sub>2</sub><sup>−</sup> = morpholide, piperidide, or diethylamide). Reactions with aryl thiols and secondary phosphines give the analogous adducts *cis*- and *trans*-[Os<sup>IV</sup>(tpy)(Cl)<sub>2</sub>(NS(H)(C<sub>6</sub>H<sub>4</sub>Me))] and *fac*-[Os<sup>IV</sup>(Tp)(Cl)<sub>2</sub>(NP(H)(Et)<sub>2</sub>)]. In dry CH<sub>3</sub>CN, all have an extensive multiple oxidation state chemistry based on couples from Os(VI/IV) to Os(III/II). In acidic solution, the Os(IV) adducts are protonated, e.g., *trans*-[Os<sup>IV</sup>(tpy)(Cl)<sub>2</sub>(N(H)N(CH<sub>2</sub>)<sub>4</sub>O)]<sup>+</sup>, and undergo proton-coupled electron transfer to quinone to give Os(V), e.g., *trans*-[Os<sup>V</sup>(tpy)(Cl)<sub>2</sub>(NN(CH<sub>2</sub>)<sub>4</sub>O)]<sup>+</sup> and hydroquinone. These reactions occur with giant H/D kinetic isotope effects of up to 421 based on O–H, N–H, S–H, or P–H bonds. Reaction with azide ion has provided the first example of the terminal N<sub>4</sub><sup>2−</sup> ligand in *mer*-[Os<sup>IV</sup>(bpy)(Cl)<sub>3</sub>(N<sub>α</sub>N<sub>β</sub>N<sub>γ</sub>N<sub>δ</sub>)]<sup>−</sup>. With CN<sup>−</sup>, the adduct *mer*-[Os<sup>IV</sup>(bpy)(Cl)<sub>3</sub>(NCN)]<sup>−</sup> has an extensive, reversible redox chemistry and undergoes NCN<sup>2−</sup> transfer to PPh<sub>3</sub> and olefins. Coordination to Os also promotes ligand-based reactivity. The sulfoximido complex *trans*-[Os<sup>IV</sup>(tpy)(Cl)<sub>2</sub>(NS(O)-*p*-C<sub>6</sub>H<sub>4</sub>Me)] undergoes loss of O<sub>2</sub> with added acid and O-atom transfer to *trans*-stilbene and PPh<sub>3</sub>. There is a reversible two-electron/two-proton, ligand-based acetonitrile/imino couple in *cis*-[Os<sup>IV</sup>(tpy)(NCCH<sub>3</sub>)(Cl)(*p*-NSC<sub>6</sub>H<sub>4</sub>Me)]<sup>+</sup>. It undergoes reversible reactions with aldehydes and ketones to give the corresponding alcohols.

## I. Introduction

In an extraordinary series of papers for their time, in the 1940s, 1950s, and 1960s, the Australian coordination chemist, Frances P. Dwyer, and a series of very talented collaborators including Alan Sargeson, David Buckingham, Harold Goodwin, and Bryce Bosnich developed the synthetic

chemistry of polypyridyl complexes of ruthenium and osmium.<sup>1</sup> Starting in the late 1960s and early 1970s, my group at the University of North Carolina began a systematic investigation of the redox reactivity of these complexes. They are typically substitutionally inert, but with the synthetic procedures from the Dwyer years in hand, it was possible to create families of related complexes in which properties could be varied by changing the ligands.

\* Author to whom correspondence should be addressed. Present affiliation: Los Alamos National Laboratory. E-mail: tjmeyer@lanl.gov.

<sup>†</sup> Los Alamos National Laboratory.

<sup>‡</sup> The University of North Carolina at Chapel Hill.

(1) Dwyer, F. P. J.; Mellor, D. P. *Chelating agents and metal chelates*; New York: Academic Press: 1964.



Thomas J. Meyer joined Los Alamos National Laboratory as Associate Director for Strategic Research in January 2000 from the University of North Carolina at Chapel Hill. At Los Alamos, Meyer is responsible for the oversight and management of SR's 2000 people, an annual budget of nearly \$400 million, and research activities that support the Laboratory's nuclear weapons and threat reduction missions. SR scientists, spanning fields from theory to bioscience, also contribute to basic and applied research in a variety of areas including energy and environment, materials, and modeling and simulation. At LANL, he also oversees industrial interactions and the Laboratory's intellectual property portfolio, the Energy and Environment Council, and LANL program offices in Science, Energy and Environment, and Nuclear Technology Applications. Meyer was a NATO postdoctoral fellow at University College, London, in 1967, joined the faculty at UNC in 1968, and was promoted to Associate Professor in 1972, Full Professor in 1975, Smith Professor in 1982, and Kenan Professor in 1987. He was the Head of Chemistry from 1985 to 1990, Chair of the Curriculum in Applied Sciences from 1994 to 1997, and Vice Chancellor and Vice Provost for Graduate Studies and Research from 1994 to 1999. He served on the North Carolina Board of Science and Technology, on the Executive Committees of the North Carolina Biotechnology Center, the Research Triangle Institute, and the Triangle University Center for Advanced Study Inc., and on the Board of Associated Universities Inc. He is currently on the Boards of the Mind Institute, the International Informatics Society, the National Center for Genome Research, the Coronado Ventures Forum, the Science and Technology External Advisory Board of Sandia National Laboratory, and the Board on Chemical Sciences and Technology of the National Research Council. Meyer is a member of the National Academy of Sciences and the American Academy of Arts and Sciences. Meyer received the 2002 ACS Award for Distinguished Service in the Advancement of Inorganic Chemistry. He has won many other awards for his research in chemistry and was awarded the Order of the Long Leaf Pine of the State of North Carolina. Meyer received his bachelor's and doctorate in chemistry from Ohio University and Stanford University, respectively. He has published over 500 papers, holds three patents, and is one of the most highly cited chemists in the world.

The reactivity properties of these complexes have turned out to be quite extraordinary based on the accessibility of long-lived excited states and oxidation states varying from M(II) to M(VI). Some of the highlights include the following:

**1. Emission, Chemiluminescence, Photophysics, and  $[\text{Ru}(\text{bpy})_3]^{2+*}$ .** Although  $[\text{Ru}^{\text{II}}(\text{bpy})_3]^{2+}$  (bpy = 2,2'-bipyridine) and related complexes are large molecules with complex electronic structures, the combination of physical measurements, theoretical interpretation, and synthetic modifications has led to an extraordinarily detailed insight into their metal-to-ligand charge-transfer (MLCT) excited states. This work has created a paradigm in molecular photochem-

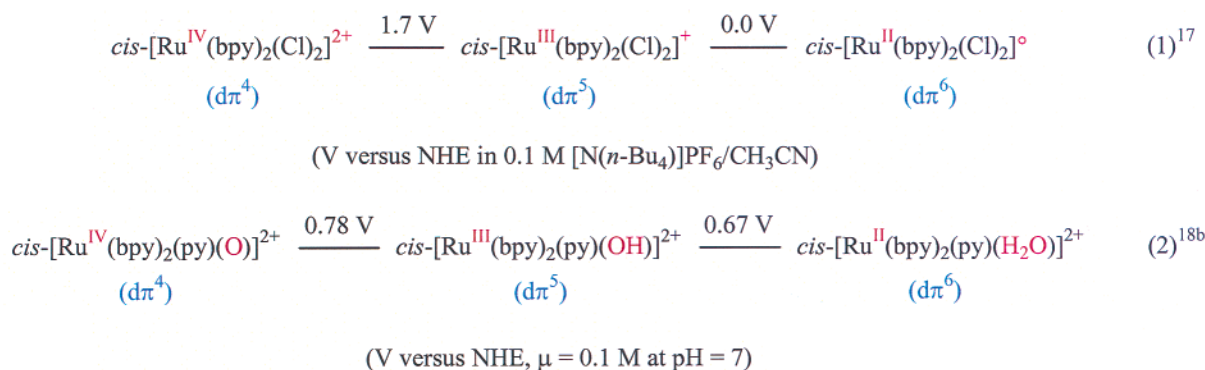
istry and applications in sensor technology and biological assays.<sup>2</sup>

**2. Photochemical Electron and Energy Transfer.** Following initial reports by Adamson and co-workers,<sup>3</sup> a series of papers appeared from the University of North Carolina in a collaborative effort with David Whitten and his group which demonstrated that  $[\text{Ru}^{\text{II}}(\text{bpy})_3]^{2+*}$  and related excited states could undergo facile oxidative and reductive electron transfer.<sup>4</sup> These early results helped to inspire a new research area, artificial photosynthesis.<sup>5,6</sup> They were also the beginning of a cottage industry in the study of photoinduced electron and energy transfer in complex molecular assemblies based on complexes of Ru(II), Os(II), and Re(I).<sup>7,8</sup> The electron-transfer properties of these excited states are also at the heart of a family of semiconductor devices based on polypyridyl complexes adsorbed to  $\text{TiO}_2$ .<sup>9,10</sup>

**3. Multielectron Reactions: The Interconversion between  $\text{NH}_3$  and  $\text{NO}_2^-$ ,<sup>11,12</sup> Reduction of  $\text{CO}_2$ ,<sup>13,14</sup> and Oxidation of  $\text{H}_2\text{O}$ .<sup>15,16</sup>** The recognition that molecular excited states could be used to create oxidative and reductive equivalents with high efficiency led to a next level of

- (2) (a) Hicks, C.; Ye, G. Z.; Levi, C.; Gonzales, M.; Rutenburg, I.; Fan, J. W.; Helmy, R.; Kassis, A.; Gafney, H. D. *Coord. Chem. Rev.* **2001**, *211*, 207–222. (b) Shan, B. Z.; Zhao, Q.; Goswami, N.; Eichhorn, D. M.; Rillema, D. P. *Coord. Chem. Rev.* **2001**, *211*, 117–144. (c) Balzani, V.; Juris, A. *Coord. Chem. Rev.* **2001**, *211*, 97–115. (d) Lee, W. Y. *Mikrochim. Acta* **1997**, *127*, 19–39.
- (3) (a) Gafney, H.; Adamson, A. W. *J. Am. Chem. Soc.* **1972**, *94*, 8238–8239. (b) Demas, J. N.; Adamson, A. W. *J. Am. Chem. Soc.* **1973**, *95*, 5159–5168; **1971**, *93*, 1800–1801.
- (4) (a) Bock, C. R.; Meyer, T. J.; Whitten, D. G. *J. Am. Chem. Soc.* **1974**, *96*, 4710–4712. (b) Young, R. C.; Meyer, T. J.; Whitten, D. G. *J. Am. Chem. Soc.* **1975**, *97*, 4781–4782. (c) Bock, C. R.; Meyer, T. J.; Whitten, D. G. *J. Am. Chem. Soc.* **1975**, *97*, 2909–2911.
- (5) (a) Meyer, T. J. *Acc. Chem. Res.* **1989**, *22*, 163–170. (b) Meyer, T. J. *Carbon Dioxide Fixation and Reduction in Biological and Model System. Proceedings of the Royal Swedish Academy of Sciences, Nobel Symposia*; Brändén, C.-I., Schneider, G., Eds.; Oxford University Press: Oxford, 1994; Chapter 14, pp 211–224.
- (6) (a) Meijer, M. D.; Van Klink, G. P. M.; Van Koten, G. *Coord. Chem. Rev.* **2002**, *230*, 141–163. (b) Durr, H.; Bossmann, S. *Acc. Chem. Res.* **2001**, *34* (11), 905–917. (c) Sun, L. C.; Hammarstrom, L.; Akermark, B.; Styring, S. *Chem. Soc. Rev.* **2001**, *30*, 36–49. (d) Gust, D.; Moore, T. A.; Moore, A. L. *Acc. Chem. Res.* **2001**, *34* (1), 40–48. (e) BouasLaurent, H.; Castellán, A.; Desvergne, J. P.; Lapouyade, R. *Chem. Soc. Rev.* **2000**, *29*, 43–55.
- (7) (a) Meyer, T. J. *Intramolecular, Photochemical Electron and Energy Transfer, Photochemical Processes in Organized Molecular Systems. Proceedings of the Memorial Conference for the late Professor Shigeo Tazuke*, Yokohama, Japan, Sept 22–24, 1990; Honda, K., Ed.; North-Holland, Elsevier: Amsterdam, 1991; pp 133–143. (b) Meyer, T. J. *Pure Appl. Chem.* **1990**, *62*, 1003–1009.
- (8) (a) Qu, P.; Thompson, D. W.; Meyer, G. J. *Langmuir* **2000**, *16* (10), 4662–4671. (b) Keene, F. R. *Coord. Chem. Rev.* **1997**, *166*, 121–159. (c) Schoonover, J. R.; Bignozzi, C. A.; Meyer, T. J. *Coord. Chem. Rev.* **1997**, *165*, 239–266. (d) Rillema, D. P.; Blanton, C. B.; Shaver, R. J.; Jackman, D. C.; Boldaji, M.; Bundy, S.; Worl, L. A.; Meyer, T. J. *Inorg. Chem.* **1992**, *31*, 1600–1606.
- (9) (a) Grätzel, M. *Curr. Opin. Colloid Interface Sci.* **1999**, *4* (4), 314–321. (b) Kalyanasundaram, K.; Grätzel, M. *Coord. Chem. Rev.* **1998**, *177*, 347–414. (c) Gerfin, T.; Grätzel, M.; Walder, L. *Prog. Inorg. Chem.* **1997**, *44*, 345–393. (d) Hagfeldt, A.; Grätzel, M. *Chem. Rev.* **1995**, *95*, 49–68.
- (10) (a) Bak, T.; Nowotny, J.; Rekas, M.; Sorrell, C. C. *Int. J. Hydrogen Energy* **2002**, *27*, 991–1022. (b) Burgeth, G.; Kisch, H. *Coord. Chem. Rev.* **2002**, *230*, 41–47. (c) Rajeshwar, K.; de Tacconi, N. R.; Chenthamarakshan, C. R. *Chem. Mater.* **2001**, *13* (9), 2765–2782. (d) Kelly, C. A.; Meyer, G. J. *Coord. Chem. Rev.* **2001**, *211*, 295–315. (e) Garcia, C. G.; deLima, J. F.; Iha, N. Y. M. *Coord. Chem. Rev.* **2000**, *196*, 219–247.
- (11) Murphy, W. R., Jr.; Takeuchi, K. J.; Meyer, T. J. *J. Am. Chem. Soc.* **1982**, *104*, 5817–5819.
- (12) Moyer, B. A.; Meyer, T. J. *J. Am. Chem. Soc.* **1979**, *101*, 1326–1328.

## Scheme 1



thinking. How do you exploit these solar energy related, one-electron processes to reactions such as H<sub>2</sub>O oxidation and CO<sub>2</sub> reduction that are multielectron in nature? Those interests led to a series of papers on H<sub>2</sub>O oxidation and CO<sub>2</sub> reduction. The observation that NH<sub>3</sub> and NO<sub>2</sub><sup>−</sup> could be rapidly and reversibly interconverted suggested possible models for important enzymatic processes such as nitrite reductase.

**4. Ru(IV) Oxo and Ru(VI) Dioxo Complexes.** These complexes are remarkably versatile oxidants mechanistically in providing pathways for atom transfer, C–H insertion, and proton-coupled electron transfer.

**5. Os(VI) Nitrido Complexes.** An even more versatile reactivity is evolving from high oxidation state nitrido complexes based on N<sup>−</sup> transfer and the redox properties of the products that result.

A full list of reactivity for these complexes is long and has been growing, which imposes demands on what can be covered in this brief account. We will focus here on two parts of the larger story. The first will be a largely retrospective look at the reactivity of ruthenium oxo complexes. The second will be on a reactivity that begins with osmium nitrido complexes and then blossoms in ways that are quite remarkable.

## II. Results and Discussion

**1. Oxidation–Reduction Chemistry.** Latimer diagrams summarizing reduction potentials and electronic configurations for two sets of Ru polypyridyl based redox couples are shown in eqs 1 and 2 (Scheme 1). The added electronic configurations make an important point. In these couples, electrons are gained and lost from dπ levels. Changes in electron content do not occur in the σ-bonding framework. This is the reason for coordinative stability in three adjacent oxidation states and explains why these complexes have been so valuable in the study of electron transfer and redox reactions in general.

The example shown in eq 1 is typical for Ru polypyridyl couples with oxidation of Ru(II) to Ru(III) occurring at easily accessible potentials. The 1.7 V increase in potential for the Ru(IV/III) couple is due to the increase in charge and oxidation state compared to the Ru(III/II) couple.<sup>17</sup>

In the couples shown in eq 2, the anionic Cl<sup>−</sup> ligands are replaced by the neutral pyridine (py) and H<sub>2</sub>O ligands. The increase in charge and changes in bonding increase the potential for oxidation of *cis*-[Ru<sup>II</sup>(bpy)<sub>2</sub>(py)(H<sub>2</sub>O)]<sup>2+</sup> (Ru<sup>II</sup>–OH<sub>2</sub><sup>2+</sup>) to *cis*-[Ru<sup>III</sup>(bpy)<sub>2</sub>(py)(OH)]<sup>2+</sup> (Ru<sup>III</sup>–OH<sup>2+</sup>) by over 0.6 V.<sup>18</sup> The potential for oxidation to the aqua complex Ru<sup>III</sup>–OH<sub>2</sub><sup>3+</sup> based on the Ru<sup>III</sup>–OH<sub>2</sub><sup>3+</sup>/Ru<sup>II</sup>–OH<sub>2</sub><sup>2+</sup> couple is even higher, 1.06 V. However, at pH 7 the relevant couple is Ru<sup>III</sup>–OH<sup>2+</sup>/Ru<sup>II</sup>–OH<sub>2</sub><sup>2+</sup>. The acidity of the Ru<sup>III</sup>–OH<sub>2</sub><sup>3+</sup> form is greatly enhanced compared to Ru<sup>II</sup>–OH<sub>2</sub><sup>2+</sup>, pK<sub>a</sub> = 0.85, and the hydroxo complex Ru<sup>III</sup>–OH<sup>2+</sup> is the dominant form at pH 7.<sup>18b</sup>

The big surprise in eq 2 is the much smaller difference between the Ru(IV/III) and Ru(III/II) couples, 0.11 V compared to 1.7 V. These data point to a dramatic stabilization of Ru(IV) in the aqua-containing coordination environment.

This is caused by proton loss and electronic stabilization of the higher oxidation state by oxo formation. pK<sub>a</sub> values are 10.6 for Ru<sup>II</sup>–H<sub>2</sub>O<sup>2+</sup>, and 0.8 and >13 for the first and second protons in *cis*-[Ru<sup>III</sup>(bpy)<sub>2</sub>(py)(H<sub>2</sub>O)]<sup>3+</sup>. The Ru(IV) form exists as the oxo complex, *cis*-[Ru<sup>IV</sup>(bpy)<sub>2</sub>(py)(O)]<sup>2+</sup> (Ru<sup>IV</sup>=O<sup>2+</sup>). There is no sign of protonation at the oxo group even in strong acids.

Stabilization of Ru(IV) as the oxo complex causes the near overlap of Ru(IV/III) and Ru(III/II) potentials. There is an important implication for reactivity in this near overlap. Thermodynamically, Ru(IV) is nearly as good a two-electron oxidant as a one-electron oxidant at pH 7.

The schematic energy orbital diagram in Figure 1 illustrates the dπ<sub>Ru</sub>–2pπ<sub>O</sub> multiple-bond interaction that stabilizes Ru(IV). Also shown are the spatial characters of the dπ\* LUMO, pπ<sub>O</sub>, and the lone pairs on the sp<sup>2</sup>-hybridized O atom. They provide an electronic clue to the extensive reactivity of Ru–oxo complexes. The LUMO is dπ\*, which is largely 4d<sub>Ru</sub> in character, antibonding, and highly mixed with 2pπ<sub>O</sub>. It provides a site for initial orbital interaction

(13) Sullivan, B. P.; Bruce, M. R. M.; O'Toole, T. R.; Bolinger, C. M.; Megehee, E.; Thorp, H.; Meyer, T. J. *Electrocatalytic Carbon Dioxide Reduction. Catalytic Activation of Carbon Dioxide*; Ayers, W. M., Ed.; ACS Symposium Series 363; American Chemical Society: Washington, DC, 1988; Chapter 6, pp 52–90.

(14) Pugh, J. R.; Bruce, M. R. M.; Sullivan, B. P.; Meyer, T. J. *Inorg. Chem.* **1991**, *30*, 86–91.

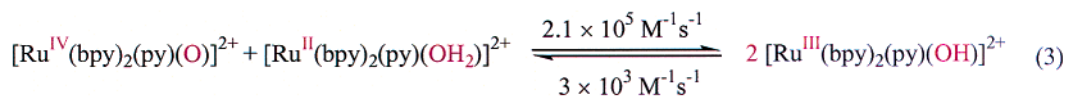
(15) Gersten, S. W.; Samuels, G. J.; Meyer, T. J. *J. Am. Chem. Soc.* **1982**, *104*, 4029–4030.

(16) Binstead, R. A.; Chronister, C. W.; Ni, J. F.; Hartshorn, C. M.; Meyer, T. J. *J. Am. Chem. Soc.* **2000**, *122*, 8464–8473.

(17) Eggleston, D. S.; Goldsby, K. A.; Hodgson, D. J.; Meyer, T. J. *Inorg. Chem.* **1985**, *24*, 4573–4580.

(18) (a) Moyer, B. A.; Meyer, T. J. *J. Am. Chem. Soc.* **1978**, *100*, 3601–3603. (b) Moyer, B. A.; Meyer, T. J. *Inorg. Chem.* **1981**, *20*, 436–444. (c) Binstead, R. A.; Moyer, B. A.; Samuels, G. J.; Meyer, T. J. *J. Am. Chem. Soc.* **1981**, *103*, 2897–2899.

## Scheme 2



$$\Delta G^\circ = -2.5 \text{ kcal mol}^{-1}$$

$$\text{Rate} = k_{\text{obs}} [\text{Ru}^{\text{IV}}=\text{O}^{2+}][\text{Ru}^{\text{II}}-\text{OH}_2^{2+}]$$

$$k_{\text{H}_2\text{O}}/k_{\text{D}_2\text{O}} = 16.1$$

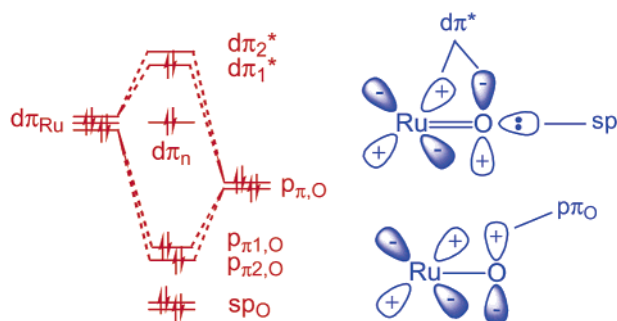
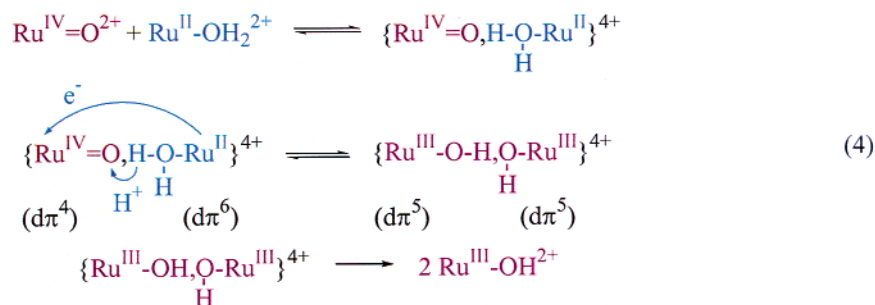


Figure 1.  $\text{Ru}^{\text{IV}}=\text{O}^{2+}$  schematic energy orbital diagram.

with electron donors. The  $sp^2$  and  $p\pi_O$  electron pairs are available for electron donation and orbital interactions with electron acceptors. The vacancy in the  $d\pi^*$  orbitals also provides a site for electron pair donation and initial coordination expansion. The  $d\pi_n$  orbitals are largely  $4d_{\text{Ru}}$  and nonbonding with regard to the  $\text{Ru}-\text{O}$   $\pi$  interaction.

**2. The Many Faces of Ruthenium Oxo Reactivity.** It was apparent from the earliest studies that polypyridyl  $\text{Ru}-\text{oxo}$  reactivity would be extraordinary. Perhaps the simplest net reaction to study is the disproportionation reaction between  $\text{Ru}^{\text{IV}}=\text{O}^{2+}$  and  $\text{Ru}^{\text{II}}-\text{OH}_2^{2+}$  to give  $\text{Ru}^{\text{III}}-\text{OH}^{2+}$  in eq 3 (Scheme 2) which occurs with  $\Delta G^\circ = -0.1 \text{ eV}$ .<sup>18</sup>

The rate constant of  $2.1 \times 10^5 \text{ M}^{-1} \text{ s}^{-1}$  is rapid, but not that rapid. Compared to related self-exchange reactions, it is slower than might have been expected by  $10^2-10^3$ .<sup>19</sup> A tip-off as to why this is so appears in the rate comparison between  $\text{H}_2\text{O}$  and  $\text{D}_2\text{O}$  which shows that the reaction is 16 times slower in  $\text{D}_2\text{O}$  than in  $\text{H}_2\text{O}$  with  $k(\text{H}_2\text{O})/k(\text{D}_2\text{O}) = 16.1$  at  $25^\circ \text{C}$ !

This was the first characterized example of *proton-coupled electron transfer*. The proposed mechanism is shown in eq 4 (Scheme 2). In it, there is an initial association between reactants, probably with hydrogen bonding between the  $\text{O}-\text{H}$

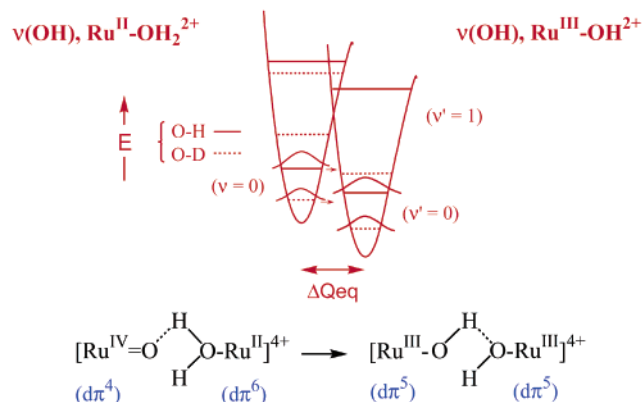


Figure 2. Intersecting  $\nu(\text{O}-\text{H})$  energy curves for proton-coupled electron transfer.

proton of the  $\text{H}_2\text{O}$  ligand in  $\text{Ru}^{\text{II}}-\text{H}_2\text{O}^{2+}$  and the oxo ligand in  $\text{Ru}^{\text{IV}}=\text{O}^{2+}$ . Association is followed by proton-coupled electron transfer which is a synchronous process with simultaneous transfer of both an electron and a proton from  $\text{Ru}^{\text{II}}-\text{H}_2\text{O}^{2+}$  to  $\text{Ru}^{\text{IV}}=\text{O}^{2+}$ . Orbitaly, the electron transfers from  $d\pi_{\text{Ru(II)}}$  to  $d\pi^*_{\text{Ru(IV)}}$  and the proton from  $\sigma_{\text{O}-\text{H}}$  to  $p\pi_{\text{O}}$  or  $sp^2_{\text{O}}$ .

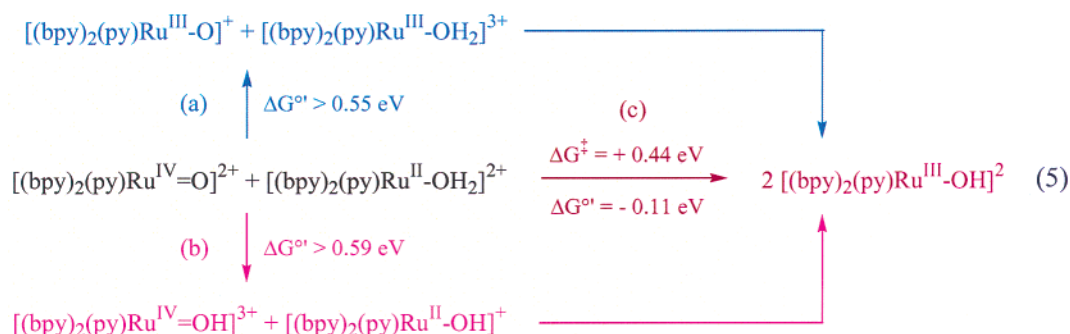
Proton-coupled electron transfer is different from H-atom transfer.<sup>20</sup> In H-atom transfer, both the electron and proton come from the same  $\text{O}-\text{H}$  bond. If H-atom transfer occurred in eq 4, it would give the intermediate  $\text{Ru}^{\text{II}}(\bullet\text{OH})^{2+}$  rather than  $\text{Ru}^{\text{III}}(\text{OH}^-)^{2+}$ . From spectroscopic measurements, a  $\text{OH}^- \rightarrow \text{Ru(III)}$  charge-transfer band is observed at 312 nm, which suggests that  $\text{Ru}^{\text{II}}(\bullet\text{OH})^{2+}$  is higher in energy by  $>2 \text{ eV}$ , ruling it out as an intermediate in the reaction.

A qualitative explanation for the large  $k_{\text{H}}/k_{\text{D}}$  isotope effect is illustrated in Figure 2. It shows the intersecting potential curves for the  $\nu(\text{O}-\text{H}), \text{Ru}^{\text{II}}-\text{OH}_2^{2+}$  and  $\nu(\text{O}-\text{H}), \text{Ru}^{\text{III}}-\text{OH}^{2+}$  normal modes that, when coupled, provide the basis for the proton-transfer part of proton-coupled electron

(19) Young, R. C.; Keene, F. R.; Meyer, T. J. *J. Am. Chem. Soc.* **1977**, *99*, 2468–2473.

(20) Binstead, R. A.; McGuire, M. E.; Dovletoglou, A.; Seok, W. K.; Roecker, L. E.; Meyer, T. J. *J. Am. Chem. Soc.* **1992**, *114*, 173–186.

Scheme 3



transfer. The constituent  $\nu(\text{O}-\text{H})$  normal modes are quantized, and vibrational wave functions are shown schematically for the  $\nu = 0, 1$  levels in the reactant and  $\nu' = 0, 1$  levels in the product. These modes have high vibrational frequencies. If only  $\nu = 0$  vibrational levels are appreciably populated at room temperature, the reactions are dominated by “nuclear tunneling” transitions from  $\nu = 0$  levels in the reactants to low-lying levels in the products. The rate contribution of each of the  $\nu \rightarrow \nu'$  vibrational channels depends on the square of their vibrational overlap integral.

As can be seen in Figure 2, the zero point energy effect of exchanging D for H places the  $\nu = 0$  energy levels lower in the vibrational potential well which decreases vibrational overlap. This feature and low thermal populations above  $\nu = 0$  play major roles in defining the reaction barrier.

Theoretical models incorporating these elements have been successfully applied to proton-coupled electron transfer by Cukier and by Hammes-Schiffer and co-workers. They have been able to calculate large kinetic isotope effects by defining appropriate coordinates and solving the Schrödinger equation to give vibrational levels and wave functions.<sup>21,22</sup> On the basis of this analysis, key parameters are the driving force and the tunneling distance ( $\Delta Q_{\text{eq}}$  in Figure 2, the distance between potential minima) since they dictate the magnitudes of the vibrational overlaps.

It is fair to ask why such a relatively complex mechanism is utilized at all. Why not electron transfer followed by proton transfer or vice versa? The answer lies in the energetics of the possible pathways shown in eq 5 at pH 7 (Scheme 3).

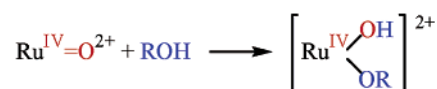
The net reaction in eq 3 requires that both an electron and a proton are transferred from  $\text{Ru}^{\text{II}}-\text{OH}_2^{2+}$  to  $\text{Ru}^{\text{IV}}=\text{O}^{2+}$ . Three possible mechanisms that do this are shown in eq 5. In reaction (a), electron transfer is followed by proton transfer. This is an accessible pathway. However, because  $\text{Ru}^{\text{III}}-\text{O}^+$  is formed without a proton and the estimated  $\text{p}K_{\text{a}}$  for  $\text{Ru}^{\text{III}}-\text{OH}^{2+}$  is  $>13$ , this pathway is uphill by at least 0.55 eV. This is the minimum free energy of activation. Its magnitude rules out a major role for this pathway since the experimental value for  $\Delta G^\ddagger$  is 0.44 eV. In reaction (b), proton transfer is followed by electron transfer. The driving force is even less favorable ( $>+0.59$  eV) due to the initial formation of protonated  $\text{Ru}^{\text{IV}}=\text{OH}^{3+}$  and deprotonated  $\text{Ru}^{\text{II}}-\text{OH}^+$ .

Because of the special orbital characteristics of  $\text{Ru}^{\text{IV}}=\text{O}^{2+}$ , which allow it to accept both an electron and a proton,

and of  $\text{Ru}^{\text{II}}-\text{OH}_2^{2+}$ , which allow it to donate both an electron and a proton, proton-coupled electron transfer in reaction (c) is orbitally accessible. It is by far the low-energy pathway, being favored by  $-0.11$  eV, and dominates reactivity in this case. Simple electron transfer is disfavored because of the thermodynamic instability of the deprotonated  $\text{Ru}^{\text{III}}-\text{O}^+$  intermediate. Proton transfer is disfavored largely because of the low affinity of the oxo group for a proton.

The orbital and energetic properties of  $\text{Ru}^{\text{IV}}=\text{O}^{2+}$  promote complex mechanisms. The driving force for  $\text{Ru}^{\text{IV}}=\text{O}^{2+}$  as a two-electron oxidant is comparable to that as a one-electron oxidant. There are  $d\pi^*$  orbitals for electronic interactions with electron donors. There are also filled  $sp^2_{\text{O}}$  and  $p\pi_{\text{O}}$  orbitals for electron pair donation to entering groups or protons as they transfer electrons to  $d\pi^*$ .

There is also the availability of a vacant  $d\pi^*$  orbital. This allows for coordination expansion by initial binding of the substrate to give seven-coordinate  $\text{Ru}(\text{IV})$  as in the oxidation of alcohols,



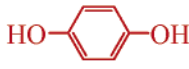
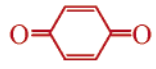
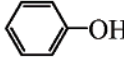
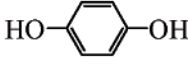
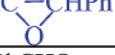

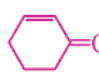

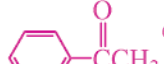
followed by intramolecular oxidation. This has been calculated to be the low-energy pathway for the stereochemically unencumbered  $\text{Ru}^{\text{IV}}=\text{O}^{2+}$  oxidant, *cis*- $[\text{Ru}^{\text{IV}}(\text{NH}=\text{CH}-\text{CH}=\text{NH}_2)(\text{NH}_3)(\text{CO})]^{2+}$  by Cundary and Drago.<sup>23</sup>

A summary of oxidative pathways for *cis*- $[\text{Ru}^{\text{IV}}(\text{bpy})_2(\text{py})(\text{O})]^{2+}$  is shown in Table 1.<sup>18,20,24–32</sup> The mechanisms cited in this table are the result of a lengthy and exhaustive series of mechanistic studies including application of global analysis techniques to transient UV–visible and infrared data, isotopic labeling, observation of intermediates, and kinetic isotope

(21) Cukier, R. I.; Nocera, D. G. *Annu. Rev. Phys. Chem.* **1998**, *49*, 337–369.  
 (22) (a) Iordanova, N.; Hammes-Schiffer, S. *J. Am. Chem. Soc.* **2002**, *124*, 4848–4856. (b) Iordanova, N.; Decornez, H.; Hammes-Schiffer, S. *J. Am. Chem. Soc.* **2001**, *123*, 3723–3733.

(23) Cundary, T. R.; Drago, R. S. *Inorg. Chem.* **1990**, *29*, 3904–3907.  
 (24) (a) Lebeau, E. L.; Binstead, R. A.; Meyer, T. J. *J. Am. Chem. Soc.* **2001**, *123*, 10535–10544. (b) Gilbert, J. A.; Gersten, S. W.; Meyer, T. J. *J. Am. Chem. Soc.* **1982**, *104*, 6872–6873. (c) Gilbert, J.; Roecker, L.; Meyer, T. J. *Inorg. Chem.* **1987**, *26*, 1126–1132.  
 (25) Seok, W. K.; Dobson, J. C.; Meyer, T. J. *Inorg. Chem.* **1988**, *27*, 3–5.  
 (26) Roecker, L.; Dobson, J. C.; Vining, W. J.; Meyer, T. J. *Inorg. Chem.* **1987**, *26*, 779–781.  
 (27) Moyer, B. A.; Sipe, B. K.; Meyer, T. J. *Inorg. Chem.* **1981**, *20*, 1475–1480.  
 (28) Stultz, L. K.; Binstead, R. A.; Reynolds, M. S.; Meyer, T. J. *J. Am. Chem. Soc.* **1995**, *117*, 2520–2532.  
 (29) Roecker, L.; Meyer, T. J. *J. Am. Chem. Soc.* **1987**, *109*, 746–754.  
 (30) Roecker, L.; Meyer, T. J. *J. Am. Chem. Soc.* **1986**, *108*, 4066–4073.  
 (31) Stultz, L. K.; Huynh, M. H. V.; Binstead, R. A.; Curry, M.; Meyer, T. J.; Bryant, J. R.; Mayer, J. M. Manuscript in preparation.  
 (32) Curry, M.; Huynh, M. H. V.; Stultz, L. K.; Binstead, R. A.; Meyer, T. J. *J. Am. Chem. Soc.* **1995**, *117*, 5984–5996.

Table 1. Mechanistic Summary for  $cis$ -[Ru<sup>IV</sup>(bpy)<sub>2</sub>(py)(O)]<sup>2+</sup>

Reduced Form	Oxidized Form	Pathway <sup>ref</sup>	$k$ (25°C) <sup>a</sup> M <sup>-1</sup> s <sup>-1</sup>	Comment
[Os <sup>II</sup> (bpy) <sub>3</sub> ] <sup>2+</sup>	[Os <sup>III</sup> (bpy) <sub>3</sub> ] <sup>3+</sup>	Outer-sphere e <sup>-</sup> transfer <sup>24a</sup>	$< 1 \times 10^3$ <b>b</b>	Slowed by initial formation of $cis$ - Ru <sup>III</sup> (bpy) <sub>2</sub> (py)(O) <sup>2+</sup>
$cis$ -[Ru <sup>II</sup> (bpy) <sub>2</sub> - (py)(OH <sub>2</sub> )] <sup>2+</sup>	$cis$ -[Ru <sup>II</sup> (bpy) <sub>2</sub> - (py)(OH)] <sup>2+</sup>	Proton-coupled e <sup>-</sup> transfer <sup>18c</sup>	$2.1 \times 10^5$ <b>b</b>	$k_{H_2O}/k_{D_2O} = 16.1$
 Hydroquinone	 Benzoquinone	Proton-coupled e <sup>-</sup> transfer <sup>20</sup>	$9.6 \times 10^5$ <b>b</b>	$k_{H_2O}/k_{D_2O} = 30$
H <sub>2</sub> O <sub>2</sub>	O <sub>2</sub>	Proton-coupled e <sup>-</sup> transfer <sup>24b-c</sup>	1.7 <b>b</b>	$k_{H_2O}/k_{D_2O} = 22$
 Phenol	 Hydroquinone <b>c</b>	Electrophilic ring attack <sup>25</sup>	$1.9 \times 10^2$	$k_H/k_D = 5.5$ (C <sub>5</sub> D <sub>5</sub> OH)
(CH <sub>3</sub> ) <sub>2</sub> S	(CH <sub>3</sub> ) <sub>2</sub> S <sub>2</sub> O	O transfer <sup>26</sup>	17	Bound sulfoxide observed
(CH <sub>3</sub> ) <sub>2</sub> SO	(CH <sub>3</sub> ) <sub>2</sub> SO <sub>2</sub>	O transfer <sup>26</sup>	0.14	
PPh <sub>3</sub>	O=PPh <sub>3</sub>	O transfer <sup>27</sup>	$1.8 \times 10^5$	Bound Ru(II) and O=PPh <sub>3</sub> observed
<i>Cis</i> -, <i>trans</i> -stilbene PhHC=CHPh	<i>cis</i> -, <i>trans</i> - PhHC-CHPh 	O transfer <sup>28</sup>	0.28, <i>trans</i> $2.5 \times 10^{-3}$ , <i>cis</i>	Bound Ru(III) epoxide observed
PhCH <sub>2</sub> OH	PhCHO	H <sup>-</sup> transfer <sup>29</sup>	2.4	$k_H/k_D = 50$
HCO <sub>2</sub> <sup>-</sup>	CO <sub>2</sub>	H <sup>-</sup> transfer <sup>30</sup>	4.2	$k_H/k_D = 19$
	 <b>d</b>	C-H insertion <sup>31</sup>	0.6	$k_H/k_D = 18$ Bound Ru(II) ketone observed
	 <b>d</b>	C-H insertion <sup>32</sup>	$6.6 \times 10^{-2}$	Bound Ru <sup>III</sup> ketone observed

<sup>a</sup> In CH<sub>3</sub>CN except where indicated. <sup>b</sup> H<sub>2</sub>O ( $\mu = 0.1$ ). <sup>c</sup> Followed by rapid oxidation to the quinone. <sup>d</sup> Through an intermediate, bound alcohol complex that undergoes further oxidation.

effects. The table lists the reductant, the oxidized product, the mechanistic pathway, rate constant information, and comments about mechanism.

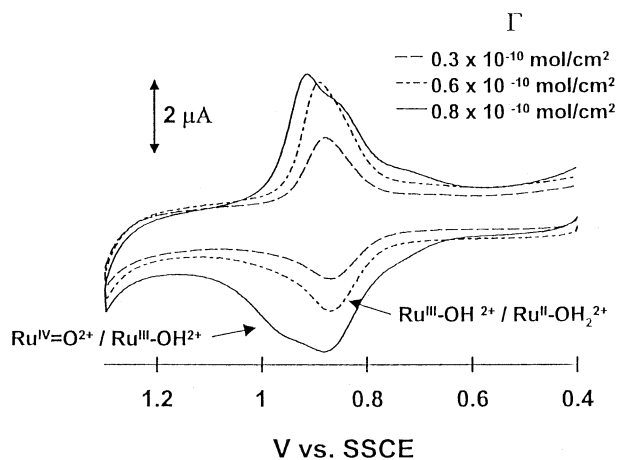
Although involving only simple electron transfer, even the first entry in Table 1 is notable.<sup>24a</sup> The reaction between Ru<sup>IV</sup>=O<sup>2+</sup> and Os<sup>II</sup>(bpy)<sub>3</sub><sup>2+</sup> is constrained to occur by outer-sphere electron transfer since there is no low-lying orbital basis for interacting in other ways. Compared to related reactions where there is no proton demand, this reaction is surprisingly slow. As in eq 5(a), this is due to the uphill nature of the initial reduction to give Ru<sup>III</sup>-O<sup>2+</sup>. Related observations have been made at electrodes where couples involving oxo complexes tend to be kinetically slow because outer-sphere electron transfer is the only available pathway.<sup>24a</sup>

Another notable reaction is with hydroquinone (H<sub>2</sub>Q) which occurs by proton-coupled electron transfer and is characterized by a H<sub>2</sub>O/D<sub>2</sub>O kinetic isotope effect of 30.<sup>20</sup> In this case, the electron comes from a molecular orbital delocalized over the aromatic ring and the electron from the O-H bond. Although initially discussed as an example of H-atom transfer,<sup>24b,c</sup> the oxidation of H<sub>2</sub>O<sub>2</sub> is more appropriately described as proton-coupled electron transfer with

the electron coming from an antibonding peroxide orbital. Another notable reaction is oxygen-atom transfer to dimethyl sulfide (SMe<sub>2</sub>), to give first the sulfoxide (S(O)Me<sub>2</sub>) and then the sulfone (S(O)<sub>2</sub>(Me)<sub>2</sub>).<sup>26</sup> Oxygen transfer and epoxidation of double bonds occur if there are no  $\alpha$  C-H bonds, as shown by the stilbene example in Table 1.<sup>28</sup> Oxidation of benzyl alcohol is listed as occurring by hydride transfer. Pathways involving C-H insertion and/or coordination expansion may also play an important role.<sup>23,37</sup>

In the oxidation of cyclohexene, a Ru(III) intermediate is observed. The  $\alpha$  C-H  $k_H/k_D$  kinetic isotope effect is 18, and a C-H insertion mechanism has been proposed.<sup>31</sup> The final product is the four-electron-oxidized ketone rather than the two-electron-oxidized alcohol. In this case, oxidation occurs by initial C-H insertion to give a bound alcohol intermediate which undergoes further rapid oxidation by a second Ru<sup>IV</sup>=O<sup>2+</sup> oxidant. As discussed in the next section, it is possible to avoid such "overoxidation" on surfaces where the Ru<sup>IV</sup>=O<sup>2+</sup> complex is the limiting reagent, and the oxidant is absorbed and translationally immobile.

**3. Reactivity on Surfaces.** The reactivity of Ru<sup>IV</sup>=O<sup>2+</sup> complexes has been explored on surfaces in electropo-



**Figure 3.** Cyclic voltammograms of  $[\text{Ru}(\text{tpy})(4,4'-(\text{PO}_3\text{H}_2)_2\text{bpy})(\text{H}_2\text{O})]-(\text{ClO}_4)_2$  adsorbed on ITO in 0.1 M  $\text{HClO}_4$  at a scan rate of 10 mV/s and at surface coverages of  $\Gamma = 0.3 \times 10^{-10}$ ,  $0.6 \times 10^{-10}$ , and  $0.8 \times 10^{-10}$ . The latter represents complete coverage.

lymerized thin polymeric films<sup>33</sup> and in monolayers on oxide surfaces.<sup>34</sup>

An example of the latter is shown in Figure 3. It is a sequence of three cyclic voltammograms. All are of the derivative  $[\text{Ru}^{\text{II}}(\text{tpy})(4,4'-(\text{PO}_3\text{H}_2)_2\text{bpy})(\text{H}_2\text{O})]^{2+}$  ( $\text{tpy} = 2,2':6',2''$ -terpyridine) adsorbed on a Sn(IV) doped  $\text{In}_2\text{O}_3$  (ITO) optically transparent electrode. The phosphonate groups at the 4- and 4'-positions of bpy form relatively stable chemical links to the surface in acidic aqueous solutions.

By controlling the time of exposure of the complex in solution to the surface, it is possible to vary surface loading. The dashed line in Figure 3 is a voltammogram of a surface with surface coverage  $\Gamma = 0.3 \times 10^{-10}$  mol/cm<sup>2</sup>. In this voltammogram, the wave observed at  $E_{1/2} = 0.86$  V at pH 1 with the characteristic splitting of  $\sim 0$  V between the oxidative and reductive waves for a surface couple appears for Ru(III/II). There is no wave for the expected Ru(IV/III) couple at higher potential. As shown by the dashed-dotted line, increasing the surface coverage by a factor of 2 causes the expected increase in Ru(III/II) peak current, but there is still no obvious Ru(IV/III) wave. Only on a fully loaded surface ( $\Gamma = 0.8 \times 10^{-10}$  mol/cm<sup>2</sup>), illustrated by the solid line, is the Ru(IV/III) wave observed.

An explanation for this phenomenon is suggested in Figure 4. On the surface, the individual adsorbed sites are translationally immobile. The only pathway for accessing  $\text{Ru}^{\text{IV}}=\text{O}^{2+}$  is by one-electron oxidation of adsorbed  $\text{Ru}^{\text{III}}-\text{OH}^{2+}$  to  $\text{Ru}^{\text{IV}}=\text{OH}^{3+}$  (reaction (a)) which occurs past the 1.6 V solvent limit in 0.1 M acid.

When the surface is fully covered with adsorbed complex, the  $\text{Ru}^{\text{III}}-\text{OH}^{2+}$  sites are sufficiently close that  $\text{Ru}^{\text{IV}}=\text{O}^{2+}$  is accessible by proton-coupled electron transfer (reaction (b)). This gives surface-bound  $\text{Ru}^{\text{IV}}=\text{O}^{2+}$  and  $\text{Ru}^{\text{II}}-\text{OH}_2^{2+}$ . The latter then undergoes fast electron transfer to give  $\text{Ru}^{\text{III}}-\text{OH}_2^{3+}$  followed by proton transfer to give  $\text{Ru}^{\text{III}}-\text{OH}^{2+}$ . The tunneling distance on the surface for proton-coupled electron transfer is apparently large since experiments with added  $\text{D}_2\text{O}$  suggest a kinetic isotope effect that exceeds 70.

An additional series of experiments has been carried out with the same adsorbed  $\text{Ru}^{\text{IV}}=\text{O}^{2+}$  oxidant but on optically transparent nanoparticles of  $\text{TiO}_2$  on glass or ITO substrates.<sup>35</sup> The resulting films are relatively thick, typically 2–8  $\mu\text{m}$ , and monolayer coverages are sufficient to use UV–visible measurements to study the kinetics of  $\text{Ru}^{\text{IV}}=\text{O}^{2+}$  reactions on the surface. Such studies have revealed important mechanistic details that were not available from studies in solution. They have also shown that surface confinement provides a way to control product selectivity.

An example is the oxidation of cyclohexene by adsorbed  $\text{Ru}^{\text{IV}}=\text{O}^{2+}$ . UV–visible measurements reveal an intermediate that is formed with a rate constant comparable to the rate constant for oxidation of cyclohexene in  $\text{CH}_3\text{CN}$  solution. The spectrum of the intermediate is consistent with C–H insertion and formation of the alcohol complex shown in eq 6 (Scheme 4). The rate constants are average values since site heterogeneities on the surface cause a distribution of reactivities.

The insertion step is followed by solvolysis to give a surface-bound solvento complex and the two-electron alcohol product. As noted above, in solution the initially formed alcohol intermediate undergoes rapid further oxidation by  $\text{Ru}^{\text{IV}}=\text{O}^{2+}$ , and the corresponding ketone is the product. The key to the apparent change in mechanism is that the oxidant is translationally confined to the surface. Once the alcohol complex is formed, it is protected from further oxidation by a second  $\text{Ru}^{\text{IV}}=\text{O}^{2+}$ .

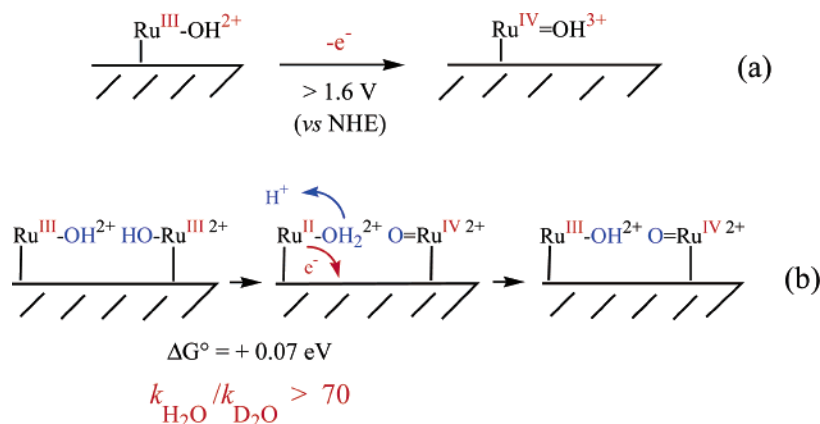
**4. Multiple Oxo Reagents and Water Oxidation.** It is also possible to access the even higher oxidation state Ru(VI) in dioxo complexes. An example is shown in Figure 5, which illustrates the structure of the cation  $\text{trans}-[\text{Ru}^{\text{VI}}(\text{tpy})(\text{O})_2(\text{H}_2\text{O})]^{2+}$ . It is formed by the  $4e^-/4\text{H}^+$  oxidation of the corresponding triaqua complex,  $\text{fac}-[\text{Ru}^{\text{II}}(\text{tpy})(\text{H}_2\text{O})_3]^{2+}$ .<sup>36,37</sup> As can be seen in the crystal structure, the Ru–O(1) and Ru–O(2) bond distances are short (1.661 and 1.662 Å), consistent with Ru–O multiple bonding. The remaining Ru–O bond length of 2.128 Å is typical for a Ru–OH<sub>2</sub> bond. The schematic orbital energy level diagram shown in Figure 5 also illustrates the combination of  $p_{\pi,\text{O}}$  with two of the  $d\pi$  orbitals at the metal to create the trans Ru–O bonding framework.

This analysis explains the preference for a *trans*-dioxo geometry compared to *cis*. The electron pair of  $d^2$  Ru(VI) is in a nonbonding orbital with regard to the Ru–O  $\pi$  interaction. The LUMOs are largely  $d\pi_{\text{Ru}}$  in character but antibonding due to  $d\pi-p_{\pi,\text{O}}$  mixing with the oxo ligands. The  $d\pi^*_{\text{Ru}}$  orbitals provide the orbital basis for the initial electron pair interaction with reducing sites such as the C–H bonding pair in benzyl alcohol<sup>37</sup> or the P-based lone pair in triarylphosphines, see below.<sup>38</sup> They also provide the basis for coordination expansion.<sup>37</sup>

The reasons for the interest in Ru–dioxo complexes are their implied ability to act as net four-electron oxidants and potential double oxygen atom transfer reagents. It is not obvious that a reasonable mechanistic pathway exists for the

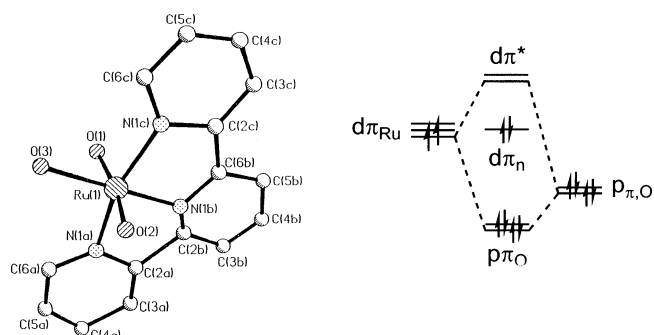
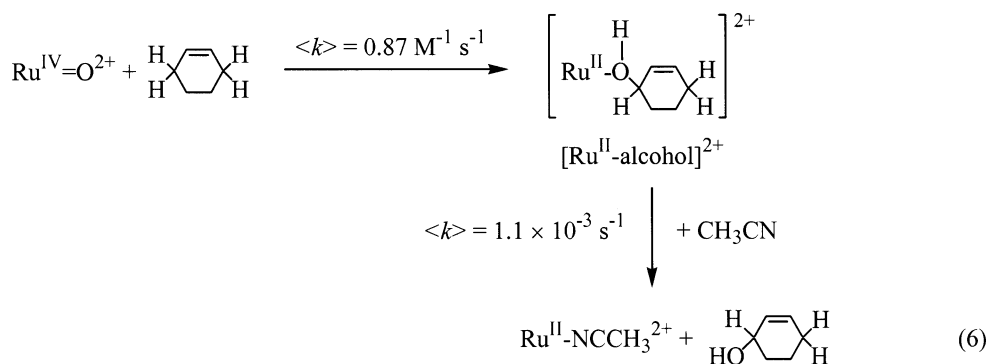
(33) (a) Leasure, R. M.; Moss, J. A.; Meyer, T. J. *Inorg. Chem.* **1994**, *33*, 1247–1248. (b) Guadalupe, A. R.; Chen, X.; Sullivan, B. P.; Meyer, T. J. *Inorg. Chem.* **1993**, *32*, 5502–5512.  
(34) Trammell, S. A.; Wimbish, J. C.; Odobel, F.; Gallagher, L. A.; Narula, P. M.; Meyer, T. J. *J. Am. Chem. Soc.* **1998**, *120*, 13248–13249.

(35) Gallagher, L. A.; Meyer, T. J. *J. Am. Chem. Soc.* **2001**, *123*, 5308–5312.  
(36) Dovletoglou, A.; Adeyemi, S. A.; Lynn, M. H.; Hodgson, D. J.; Meyer, T. J. *J. Am. Chem. Soc.* **1990**, *112*, 8989–8990.  
(37) Lebeau, E. L.; Meyer, T. J. *Inorg. Chem.* **1999**, *38*, 2174–2181.  
(38) (a) Adeyemi, S. A.; Dovletoglou, A.; Guadalupe, A. R.; Meyer, T. J. *Inorg. Chem.* **1992**, *31*, 1375–1383. (b) Dovletoglou, A.; Meyer, T. J. *J. Am. Chem. Soc.* **1994**, *116*, 215–223.



**Figure 4.** Schematic illustration of adsorbed  $[\text{Ru}(\text{tpy})(4,4'-(\text{PO}_3\text{H}_2)_2\text{bpy})(\text{H}_2\text{O})](\text{ClO}_4)_2$  on an ITO surface showing direct oxidation and disproportionation as routes to  $\text{Ru}^{\text{IV}}=\text{O}^{2+}$ .

#### Scheme 4



**Figure 5.** ORTEP diagram and labeling scheme for the cation  $\text{trans}-[\text{Ru}^{\text{VI}}(\text{tpy})(\text{O})_2(\text{H}_2\text{O})]^{2+}$  and a schematic energy level diagram.

latter. From the structure in Figure 5, the distance spanning the trans oxo groups is 3.32 Å, seemingly too large for simple reductants to avail themselves of the di-O-atom transfer capability of the oxidant. This point was explored by studying the reactions of the dioxo complex with a series of tertiary diphosphines. The results for  $\text{Ph}_2\text{P}(\text{CH}_2)_2\text{PPh}_2$  in  $\text{CH}_3\text{CN}$  at 25 °C are summarized in eq 7 (Scheme 5).<sup>38b</sup>

Initial O-atom transfer occurs to one end of the tertiary diphosphine reductant and, from the results of a stopped-flow kinetics study, with a rate constant that is within a factor of ~10 of the diffusion-controlled limit. These studies show that the second O-atom can be used and that there are two separate pathways for using it.

In one, shown at the top of eq 7, initial O-atom transfer is followed by a rate-limiting coordination sphere rearrangement in which an interchange occurs between the second oxo ligand and a solvent molecule, in this case acetonitrile. The interchange positions the second oxo group for attack

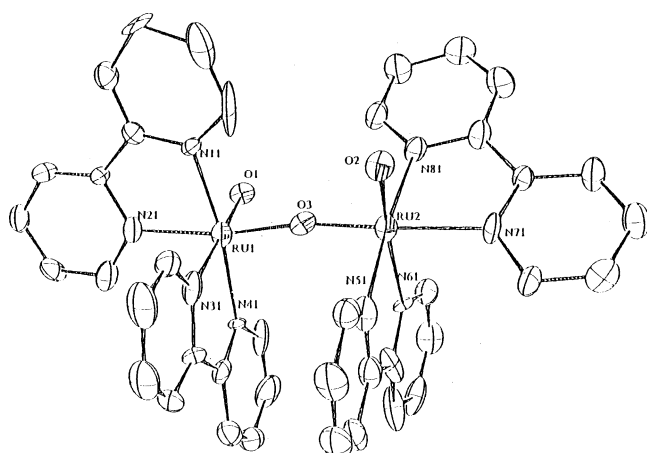
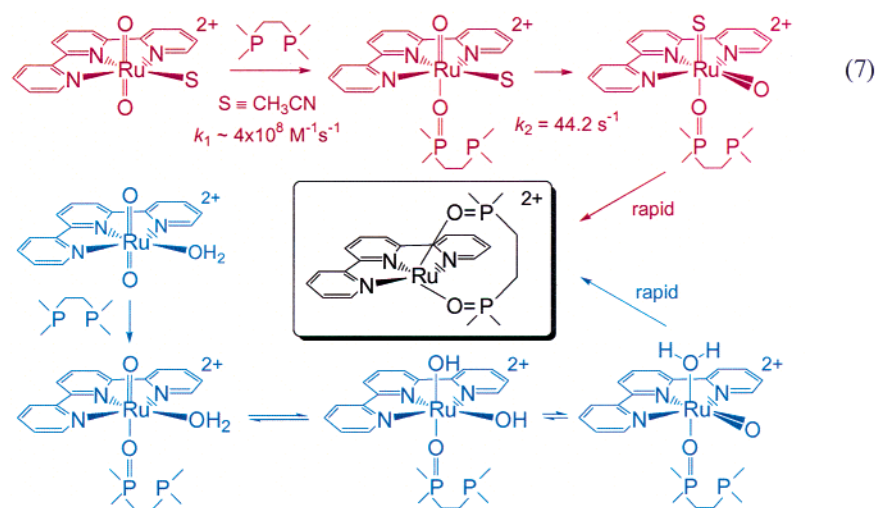
on the partly oxidized tertiary diphosphine. In contrast to  $d^2$   $\text{Ru}(\text{VI})$ , there is no strong stereochemical preference for the O-ligand in the  $d^4$  electronic configuration of the  $\text{Ru}(\text{IV})$  intermediate. The transfer between coordination sites is followed by an O-atom transfer to give the final five-coordinate  $\text{Ru}(\text{II})$  product containing the chelated tertiary diphosphine dioxide ligand.

As shown at the bottom of eq 7, with a little added water the dominant form of the dioxo complex contains bound water rather than acetonitrile in the tpy coordination plane. The first O-atom transfer is, again, very rapid, but the second oxo group is utilized in a different way. The overall rate constant for the second step is  $k'_2 = 6.2 \times 10^{-2} \text{ s}^{-1}$ , and the reaction occurs with an inverse  $k(\text{H}_2\text{O})/k(\text{D}_2\text{O})$  kinetic isotope effect of 0.2. As shown in eq 7, this has been interpreted by invoking internal proton transfer and a preequilibrium between oxo-aqua and dihydroxo forms of  $\text{Ru}(\text{IV})$ . Subsequent proton transfer in the opposite direction leads to net transfer of the oxo group to the reactive cis position and is followed by rapid oxo transfer to the second diarylphosphine group. The unusually small  $\text{H}_2\text{O}/\text{D}_2\text{O}$  inverse isotope effect arises from the oxo-aqua/dihydroxo preequilibrium. This is a vibrational partition function effect that arises from loss of a vibrational mode when the coordinated water molecule is converted into two hydroxo ligands.<sup>38b</sup>

**5. Water Oxidation.** The initial experiments that led to the discovery of polypyridyl  $\text{Ru}$ -oxo complexes and  $\text{cis}-[\text{Ru}^{\text{IV}}(\text{bpy})_2(\text{py})(\text{O})]^{2+}$  were conducted in an attempt to develop catalysts for water oxidation to  $\text{O}_2$ . The strategy was to bind a  $\text{H}_2\text{O}$  molecule in a coordination environment where multiple electron transfer could occur. This initial attempt was unsuccessful. The resulting oxo complex in eq 2 is not



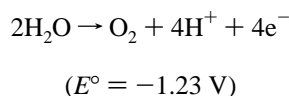
Scheme 5



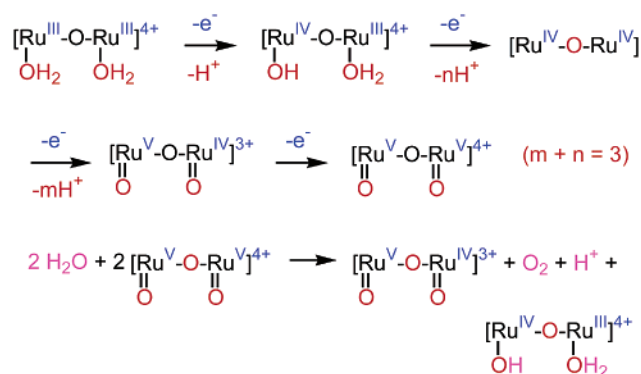
**Figure 6.** ORTEP diagram and labeling scheme for the cation  $[(bpy)_2-(H_2O)Ru^{III}-O-Ru^{IV}(OH)(bpy)_2]^{4+}$ . Data in the structure:  $Ru(1)-O = 1.847(12)$  Å,  $Ru(2)-O = 1.823(12)$  Å, and  $\angle Ru-O-Ru = 170.0(7)^\circ$ .

a catalyst for water oxidation since, over a broad pH range, it is not a sufficiently strong oxidant thermodynamically to carry out the reaction.

An obvious strategy to pursue was to design related complexes that contained chemically linked  $Ru-OH_2^{2+}$  sites. This was in recognition of the fact that water oxidation requires the loss of  $4e^-$  and  $4H^+$  with the formation of an  $O-O$  bond.



Mechanisms involving one-electron transfer are accessible but demand powerful oxidants since intermediates such as hydroxyl radical,  $\cdot OH$ , or  $H_2O^{\cdot+}$  are of high energy thermodynamically. The molecular structure of a second-generation approach to the design of water oxidation catalysts is shown in Figure 6. It is *cis,cis*- $[(bpy)_2(OH)Ru^{IV}-O-Ru^{III}(H_2O)(bpy)_2]^{4+}$ , the one-electron-oxidized form of the blue dimer precursor, *cis,cis*- $[(bpy)_2(H_2O)Ru^{III}-O-Ru^{III}(H_2O)(bpy)_2]^{4+}$ .<sup>16,39–42</sup> They are two members of the  $4e^-/4H^+$  oxidation sequence shown in Figure 7 which ultimately leads



**Figure 7.** Water oxidation mechanism for  $[(bpy)_2(H_2O)Ru^{III}-O-Ru^{III}(H_2O)(bpy)_2]^{4+}$ .

to water oxidation. This scheme was established through a series of painstaking experiments involving stopped-flow kinetics measurements and the spectroscopic identification of intermediates.<sup>16,43–45a</sup>

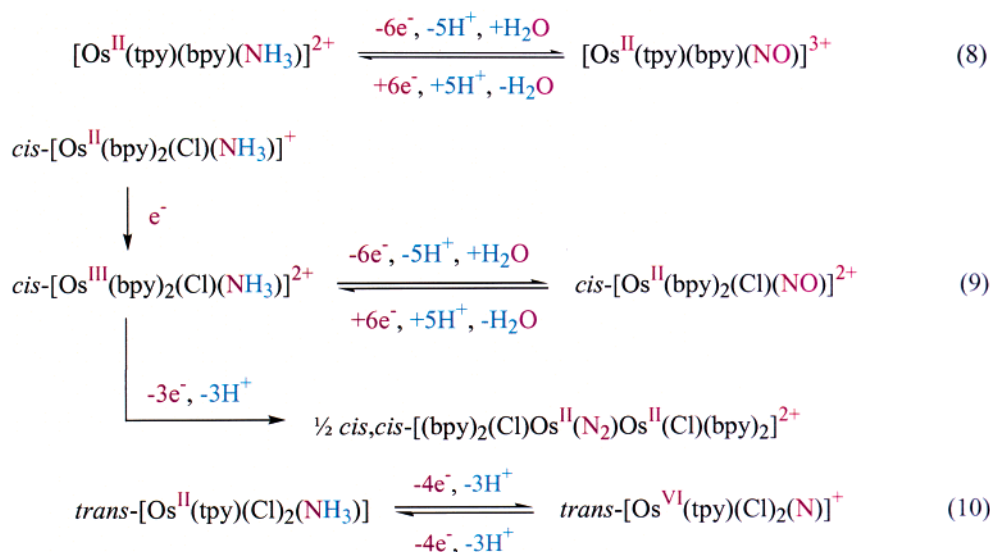
The loss of both electrons and protons in the steps of this sequence is important in meeting the overall requirements for water oxidation. Electron–proton loss from the blue dimer to give *cis,cis*- $[(bpy)_2(OH)Ru^{IV}-O-Ru^{III}(H_2O)(bpy)_2]^{3+}$  is followed by the loss of a second electron and multiple protons to give an intermediate which is formally  $Ru^{IV}-O-Ru^{IV}$ . It is thermodynamically unstable with regard to disproportionation into  $Ru^{IV}-O-Ru^{III}$  and  $Ru^V-O-Ru^{IV}$ . Further one-electron oxidation of  $Ru^{IV}-O-Ru^{IV}$  gives  $Ru^V-O-Ru^{IV}$ , which, by inference, exists as the  $\mu$ -oxo, dioxo structure suggested in Figure 7.

The reactive form of the catalyst system is  $[(bpy)_2(O)-Ru^V-O-Ru^V(O)(bpy)_2]^{4+}$ ,  $[(O)Ru^V-O-Ru^V(O)]^{4+}$  in Fig-

(39) Vining, J. W.; Meyer, T. J. *Inorg. Chem.* **1986**, *25*, 2023–2033.

(40) Bartolotti, L. J.; Pedersen, L. G.; Meyer, T. J. *Int. J. Quantum Chem.* **2001**, *83*, 143–149.  
 (41) Hurst, J. K.; Zhou, J. Z.; Lei, Y. B. *Inorg. Chem.* **1992**, *31*, 1010–1017.  
 (42) Schoonover, J. R.; Ni, J. F.; Roecker, L.; Whiter, P. S.; Meyer, T. J. *Inorg. Chem.* **1996**, *35*, 5885–5892.  
 (43) Lebeau, E. L.; Adeyemi, S. A.; Meyer, T. J. *Inorg. Chem.* **1998**, *37*, 6476–6484.  
 (44) Geselowitz, D.; Meyer, T. J. *Inorg. Chem.* **1990**, *29*, 3894–3896.  
 (45) (a) Chronister, C. W.; Binstead, R. A.; Ni, J. F.; Meyer, T. J. *Inorg. Chem.* **1997**, *36*, 3814–3815. (b) Ishitani, O.; Ando, E.; Meyer, T. J. *Inorg. Chem.* **2003**, *42*, 1707–1710.

Scheme 6



ure 7. It oxidizes  $\text{H}_2\text{O}$  to  $\text{O}_2$  on the sub-millisecond time scale as shown by stopped-flow kinetics measurements. This intermediate precipitates as the  $\text{ClO}_4^-$  salt in cold, strongly acidic solutions as a black solid. Resonance Raman measurements on the solid show that the  $\mu$ -oxo bridge remains intact and that there are terminal Ru–oxo groups. Manipulating this solid is difficult because it detonates on handling with the evolution of  $\text{O}_2$ .

The  $\mu$ -oxo blue dimer is a catalyst for the oxidation of  $\text{H}_2\text{O}$  to  $\text{O}_2$  by the strong oxidant Ce(IV). Complications exist in the catalytic cycle arising from anion binding which accompanies  $\text{O}_2$  evolution. Anion binding inhibits  $\text{O}_2$  evolution and slows the overall catalysis because the rate-limiting step becomes water replacement of the coordinated anion, and it is far slower than the water oxidation step.<sup>16</sup> This complication has limited studies on  $\text{O}_2$  evolution, but the catalyst has been shown to continue through hundreds of catalytic cycles.

Interestingly, oxidation of coordinated  $\text{NH}_3$  to  $\text{N}_2$  has been observed in the analogous dimer,  $\text{cis,cis-}[(\text{bpy})_2(\text{NH}_3)\text{Ru}^{\text{III}}-\text{O}-\text{Ru}^{\text{III}}(\text{NH}_3)(\text{bpy})_2]^{4+}$ . In this case,  $^{15}\text{N}$  labeling has shown that  $\text{N}_2$  formation occurs by intramolecular oxidative coupling.<sup>45b</sup>

**6. Oxidation of Coordinated Ammonia.** Oxo complexes are formed by oxidation and proton loss from bound aqua ligands. Reasoning by analogy, we investigated the oxidation of coordinated ammonia as a way to access high oxidation state nitrido complexes. Initial experiments in this area revealed a far more complex redox chemistry than found for coordinated water. This is illustrated by the series of reactions in eqs 8 and 9 (Scheme 6).

In the relatively electron deficient coordination environment found in  $[\text{Os}^{\text{II}}(\text{tpy})(\text{bpy})(\text{NH}_3)]^{2+}$ , initial one-electron oxidation from Os(II) to Os(III) is reversible and facile. In weakly acidic or basic solutions, further multielectron oxidation occurs to give the nitrosyl complex as shown in eq 8.<sup>46,47</sup>

This six-electron/five-proton reaction is remarkably facile. It is equally remarkable that the reaction is reversible with the coordinated nitrosyl being reduced to coordinated ammonia in acidic solution.

Exchange of an electron-donating  $\text{Cl}^-$  ligand for pyridine changes the chemistry as shown in eq 9. In this case, oxidation past Os(III) gives two products, and the distribution depends on pH. One product is the nitrosyl as in eq 8. The other is a  $\mu$ - $\text{N}_2$  bridged complex that is formed by net loss of  $3e^-/3H^+$  at two sites followed by  $\text{N}\cdots\text{N}$  coupling, eq 9.<sup>47</sup>

A N-based chemistry that parallels the aqua/oxo chemistry does appear in sufficiently electron rich coordination environments.<sup>48–51</sup> As shown in eq 10 (Scheme 6),  $\text{trans-}[\text{Os}^{\text{II}}(\text{tpy})(\text{Cl})_2(\text{NH}_3)]$  undergoes  $4e^-/3H^+$  oxidation to give the corresponding Os(VI)–nitrido product. The reaction to give back the amine complex is chemically reversible, but the interconversion is kinetically and mechanistically complex.<sup>48–51</sup>

A summary of reactions inferred by a combination of product isolation, spectroscopic, and electrochemical studies is shown in Figure 8. In this figure, Nu is an abbreviation for an electron pair donating, redox nucleophile, i.e., DMSO (see below).

In Figure 8, one-electron oxidation of  $\text{Os}^{\text{II}}-\text{NH}_3^{m+}$  to  $\text{Os}^{\text{III}}-\text{NH}_3^{(m+1)+}$  is followed by further oxidation to  $\text{Os}^{\text{IV}}-\text{NH}_3^{(m+2)+}$  with proton loss to give  $\text{Os}^{\text{IV}}-\text{NH}_2^{(m+1)+}$  or  $\text{Os}^{\text{IV}}=\text{NH}^{m+}$ . The latter is electronically analogous to an equivalent  $\text{Os}^{\text{IV}}=\text{O}^{2+}$  complex. Once formed, Os(IV) is unstable with respect to disproportionation into  $\text{Os}^{\text{III}}-\text{NH}_3^{(m+1)+}$  and  $\text{Os}^{\text{VI}}\equiv\text{N}^{(m+1)+}$ . Os(IV) can also undergo  $\text{N}\cdots\text{N}$  coupling presumably through an, as yet, unobserved diimino bridged intermediate. Further  $2e^-/2H^+$  oxidation of this intermediate leads to the  $\text{Os}^{\text{II}}-\text{N}_2-\text{Os}^{\text{II}}$  product. In the absence of protons, reduction

(46) Murphy, W. R.; Takeuchi, K. J.; Barley, M. H.; Meyer, T. J. *Inorg. Chem.* **1986**, *25*, 1041–1053.

(47) Coia, G. M.; Demadis, K. D.; Meyer, T. J. *Inorg. Chem.* **2000**, *39*, 2212–2223.

(48) Pipes, D. W.; Bakir, M.; Vitols, S. E.; Hodgson, D. J.; Meyer, T. J. *J. Am. Chem. Soc.* **1990**, *112*, 5507–5514.

(49) (a) El-Samanody, E.-S.; Demadis, K. D.; Meyer, T. J.; White, P. S. *Inorg. Chem.* **2001**, *40*, 3677–3686. (b) Huynh, M. H. V.; Meyer, T. J. Unpublished results.

(50) Coia, G. M.; Demadis, K. D.; Meyer, T. J. *Inorg. Chem.* **2000**, *39*, 2212–2223.

(51) (a) Huynh, M. H. V.; White, P. S.; John, K. D.; Meyer, T. J. *Angew. Chem., Int. Ed.* **2001**, *40*, 4049–4051. (b) Huynh, M. H. V.; Scott, B. L.; Meyer, T. J. Work in progress.

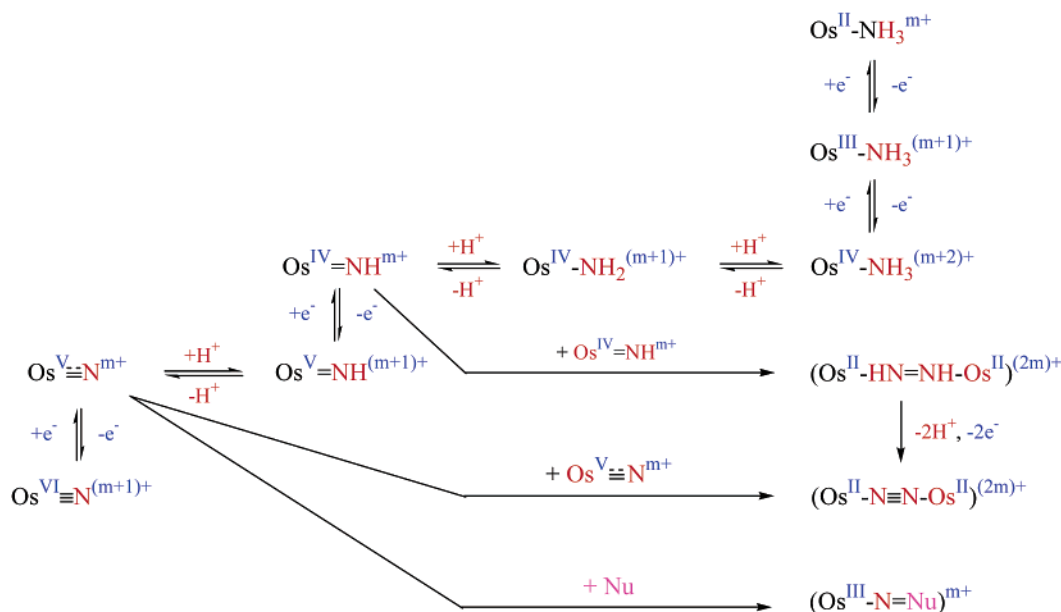


Figure 8. Oxidation–reduction and proton-transfer intermediates in the oxidation of coordinated ammonia.

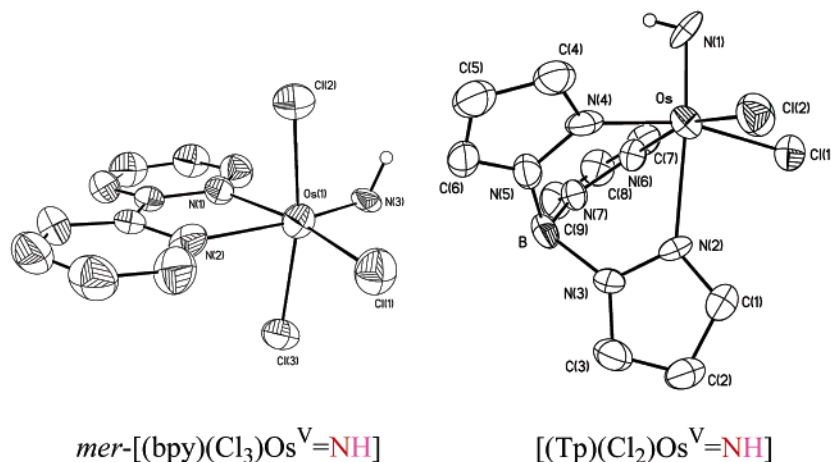


Figure 9. ORTEP diagram (30% ellipsoids) and labeling scheme for  $[\text{Os}^{\text{V}}(\text{Tp})(\text{Cl})_2(\text{NH})]$  ( $r_{\text{Os-NH}} = 1.749(7)$  Å) and  $[\text{Os}^{\text{V}}(\text{bpy})(\text{Cl})_3(\text{NH})]$  ( $r_{\text{Os-NH}} = 1.811(1)$  Å).

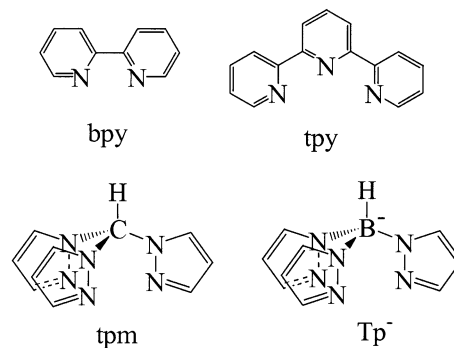
of Os(VI) to Os(V) also gives  $[\text{Os}^{\text{II}}-\text{N}_2-\text{Os}^{\text{II}}]^{(2m)+}$  dimers by  $\text{Os}^{\text{V}}\equiv\text{N}^{(m+)+}\cdots\text{N}\equiv\text{Os}^{\text{V}(m+)+}$  coupling.

Os(IV), as  $\text{Os}^{\text{IV}}-\text{NH}_2^{(m+1)+}$  or  $\text{Os}^{\text{IV}}=\text{NH}^{m+}$ , is a key intermediate. It undergoes coupling followed by oxidation to give  $\mu\text{-N}_2$  products. Further oxidation gives  $\text{Os}^{\text{V}}=\text{NH}^{(m+1)+}$ , which undergoes disproportionation to give  $\text{Os}^{\text{III}}-\text{NH}_3^{(m+1)+}$  and  $\text{Os}^{\text{VI}}\equiv\text{N}^{(m+1)+}$ .

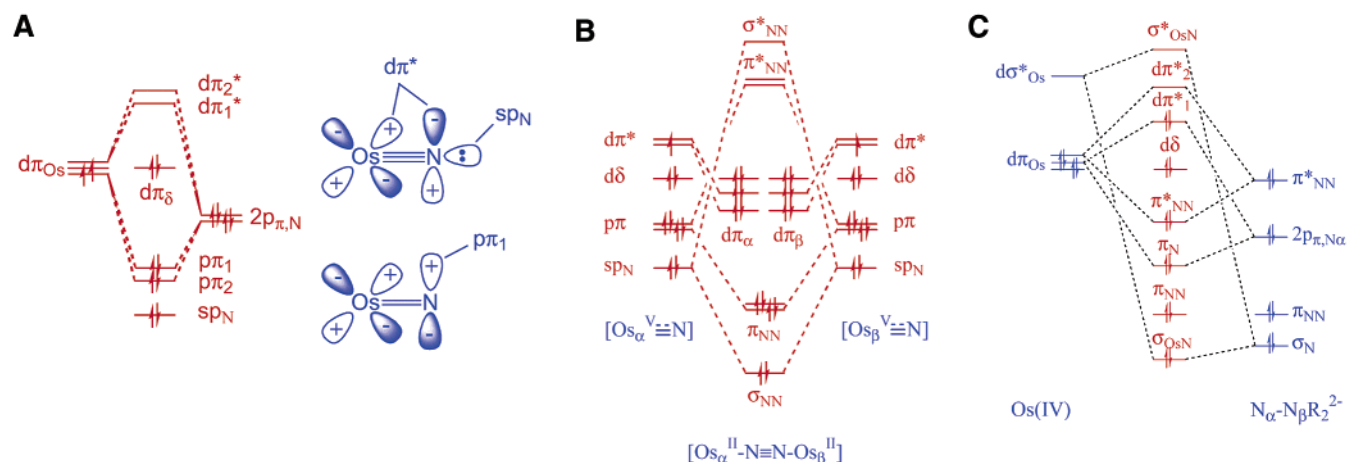
Even given its instability with respect to disproportionation, examples of  $\text{Os}^{\text{V}}=\text{NH}^{(m+1)+}$  have been isolated and crystallized in strongly acidic, mixed-solvent environments.<sup>51</sup> Crystal structures of two examples are shown in Figure 9. The structures reveal relatively short Os–N bonds, 1.749–(7) Å for *fac*- $[\text{Os}^{\text{V}}(\text{Tp})(\text{Cl})_2(\text{NH})]$  and 1.811(1) Å for *mer*- $[\text{Os}^{\text{V}}(\text{bpy})(\text{Cl})_3(\text{NH})]$ , consistent with Os–N multiple bonding.

**7. Reactivity of Os(VI) Nitrido Complexes.** There is an impressive redox reactivity of Os(VI)–nitrido complexes, and it continues to evolve. It is based on a series of complexes in which electron content is varied systematically by varying the ligands. Examples, along with irreversible cathodic peak potentials for  $\text{Os}^{\text{VI}} + e^- \rightarrow \text{Os}^{\text{V}}$  couples (in DMF at 25 °C, V versus SSCE), are  $E_{\text{pc}} = -0.28$  and  $-0.41$

V for *cis*- and *trans*- $[\text{Os}^{\text{VI}}(\text{tpy})(\text{Cl})_2(\text{N})]^+$ ,  $E_{\text{pc}} = -0.47$  V for *fac*- $[\text{Os}^{\text{VI}}(\text{tpm})(\text{Cl})_2(\text{N})]^+$  (tpm = tris(pyrazol-1-yl)methane),  $E_{\text{pc}} = -0.98$  V for *fac*- $[\text{Os}^{\text{VI}}(\text{Tp})(\text{Cl})_2(\text{N})]$  (Tp = tris(pyrazol-1-yl)borate), and  $E_{\text{pc}} = -1.11$  V for *mer*- $[\text{Os}^{\text{VI}}(\text{bpy})(\text{Cl})_3(\text{N})]$ .<sup>51</sup> The structures of the chelate ligands are illustrated below.

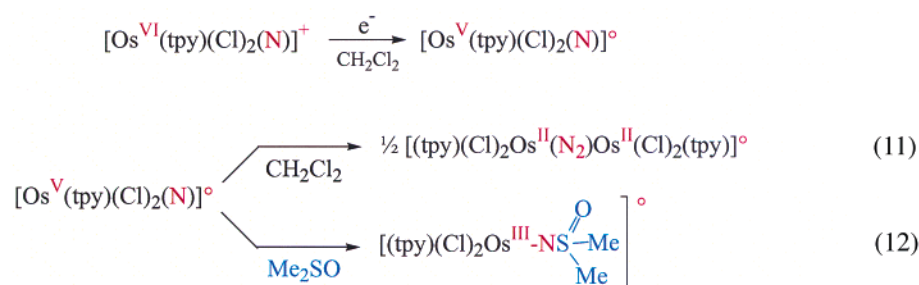


The  $E_{\text{pc}}$  values provide a relative measure of oxidizing ability of the complexes, and the range of values from  $-0.28$



**Figure 10.** Schematic energy level diagrams illustrating (A) the bonding in Os(VI)-nitrido complexes; (B) the change in bonding that occurs upon dimerization of Os(V)-nitrido to give Os<sup>II</sup>-N≡N-Os<sup>II</sup>; and (C) schematic energy level diagram for Os<sup>IV</sup>-NNR<sub>2</sub> (taken from ref 51).

### Scheme 7



to  $-1.11$  V illustrates the influence of ligand variations on electron content at Os<sup>VI</sup>≡N. Exchanging electron donor anionic Cl<sup>-</sup> or Tp<sup>-</sup> ligands for neutral terpyridine (tpy) or tris(pyrazol-1-yl)methane (tpm) ligands decreases electron content and increases oxidative reactivity. In the series, *trans*-[Os<sup>VI</sup>(tpy)(Cl)<sub>2</sub>(N)]<sup>+</sup> is the most reactive and *mer*-[Os<sup>VI</sup>(bpy)(Cl)<sub>3</sub>(N)] the least toward nucleophilic electron donors.

Much of the redox reactivity that has been observed can be anticipated by considering the schematic energy level diagram in Figure 10A. It illustrates the  $d\pi$ - $p\pi$  interactions that exist between the 5d- $d\pi$ (Os) orbitals and the two  $p\pi$  orbitals on N. This results in two  $p\pi$  levels that are bonding and largely N in character. When combined with the Os-N  $\sigma$  bond, they provide the orbital basis for the triple-bond interaction between Os and N. The third 2p<sub>N</sub> orbital is hybridized with 2s and 2p<sub>s</sub> to create an sp lone pair localized on the nitrido ligand. Assuming the z-axis to fall along the Os-N bond, there is a filled d<sub>xy</sub> orbital that has  $\delta$  symmetry with regard to the Os-N interaction and is doubly occupied. The LUMOs are  $d\pi^*$  orbitals which are antibonding and largely  $d\pi_{\text{Os}}$  in character. They are available for accepting electrons or electron pairs from reducing agents.

As in the Ru<sup>IV</sup>=O<sup>2+</sup> complexes, there is also a possibility of coordination expansion by using the  $d\pi^*$  orbitals. Addition of the reducing agent would give seven-coordinate Os(VI) and the final product by intramolecular coupling.

In CH<sub>2</sub>Cl<sub>2</sub>, which acts as an inert solvent, one-electron reduction of *trans*-[Os<sup>VI</sup>(tpy)(Cl)<sub>2</sub>(N)]<sup>+</sup> gives *trans*-[Os<sup>V</sup>(tpy)(Cl)<sub>2</sub>(N)] as a transient.<sup>48,49</sup> In the absence of protons, the Os(V)-nitrido intermediate is unstable toward N $\cdots$ N coupling and formation of *trans,trans*-[(tpy)(Cl)<sub>2</sub>Os<sup>II</sup>(N<sub>2</sub>)Os<sup>II</sup>(Cl)<sub>2</sub>(tpy)], eq 11 (Scheme 7).<sup>49</sup> One-electron reduction

occurs at  $d\pi_1^*$ , and this weakens the Os-N interaction and promotes N $\cdots$ N coupling.

N $\cdots$ N coupling of [Os<sup>V</sup>(NH<sub>3</sub>)<sub>4</sub>(N)]<sup>2+</sup>, generated by laser flash photolysis of [Os<sup>VI</sup>(NH<sub>3</sub>)<sub>4</sub>(N)]<sup>3+</sup> in the presence of electron donors such as 1,4-dimethoxybenzene, has been shown to be rapid,  $k(\text{CH}_3\text{CN}, 25^\circ\text{C}) = (3.75 \pm 0.30) \times 10^5 \text{ dm}^3 \text{ mol}^{-1} \text{ s}^{-1}$ .<sup>52</sup>

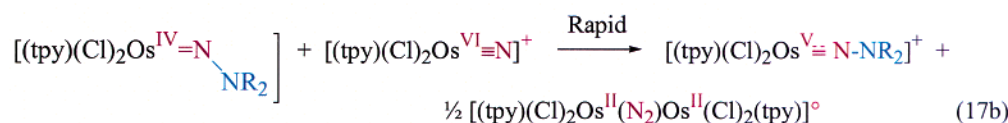
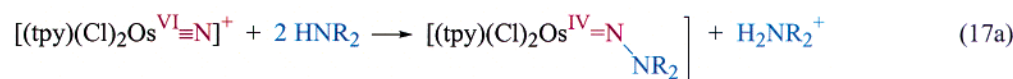
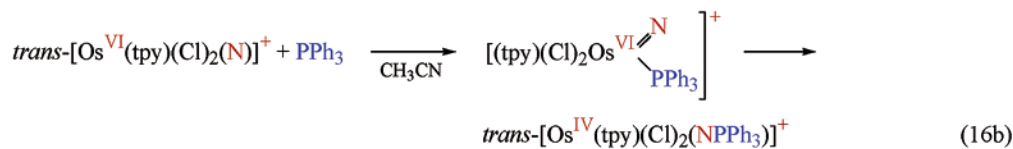
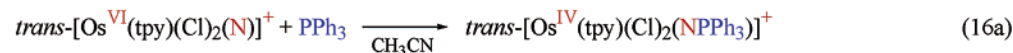
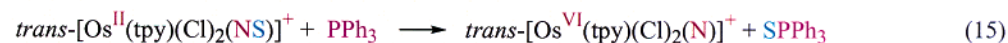
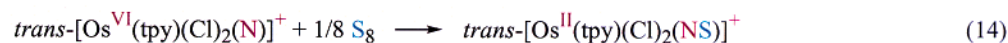
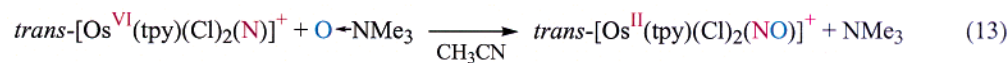
As shown in the schematic orbital correlation diagram in Figure 10B, N $\cdots$ N coupling leads to a significant change in bonding and relative orbital energies, and extensive internal electronic redistribution. It results in reduction in oxidation state to Os(II) and formation of a triple bond at the bridging N<sub>2</sub> ligand. The dramatic change in oxidation state at the metal is a consequence of the loss of  $d\pi$ - $p\pi$  mixing which removes the antibonding character of the  $d\pi$  orbitals.

In dimethyl sulfoxide (Me<sub>2</sub>SO) as solvent, another pathway competes for Os(V). As shown in eq 12 (Scheme 7), it involves net N<sup>-</sup> transfer to the solvent to give an Os(III)-sulfoximido product.<sup>51</sup> This reactivity is analogous to oxo transfer to Me<sub>2</sub>SO by *cis*-[Ru<sup>IV</sup>(bpy)<sub>2</sub>(py)(O)]<sup>2+</sup> in Table 1.

Reduction of Os<sup>VI</sup>≡N at  $d\pi^*$  is highly activating toward N<sup>-</sup> transfer. The Os(VI)-nitrido precursor is stable for extended periods at room temperature in Me<sub>2</sub>SO. One-electron reduction to Os(V) activates the Os-N bond toward N<sup>-</sup> transfer to Me<sub>2</sub>SO. Although this may appear counter-intuitive, it is analogous to the enhanced reactivity of one-electron organic and inorganic radicals. The key is that the added electron occupies a highly destabilized  $d\pi^*$  orbital which enhances N<sup>-</sup> transfer.

(52) Lam, H. W.; Che, C. M.; Wong, K. Y. *J. Chem. Soc., Dalton Trans.* **1992**, 8, 1411-1416.

Scheme 8



The N-based sp lone pair in  $\text{Os}^{\text{VI}} \equiv \text{N}$  provides a potential reaction site toward oxidation. A reaction does occur between  $\text{trans-}[\text{Os}^{\text{VI}}(\text{tpy})(\text{Cl})_2(\text{N})]^+$  and trimethylamine *N*-oxide ( $\text{O} \leftarrow \text{NMe}_3$ ) in  $\text{CH}_3\text{CN}$  as described in eq 13 (Scheme 8).<sup>53</sup> This is also a remarkable reaction since there is a change in oxidation state at Os from VI to II and at N from  $-3$  to  $+3$ . It is another case where atom transfer or coupling leads to a significant change in orbital energies and electronic distribution. O-atom transfer and internal electron transfer to Os results in the formation of the N–O triple bond and loss of antibonding character in the  $d\pi_{\text{Os}}$  orbitals.

The nitrido complex also undergoes a reaction with  $\text{S}_8$  to give the corresponding thionitrosyl, eq 14 (Scheme 8). The thionitrosyl, in turn, undergoes S-atom transfer in its reaction with  $\text{PPh}_3$ , eq 15 (Scheme 8).<sup>54</sup>

This reaction is also remarkable in that S-atom transfer to  $\text{PPh}_3$  is accompanied by oxidation of Os(II) to Os(VI)! It has been shown to occur through the intermediate,  $[\text{Os}^{\text{IV}}(\text{tpy})(\text{Cl})_2(\text{NSPPH}_3)]^+$ .<sup>55</sup> In an orbital sense, it can be understood by invoking initial electron pair donation from  $\text{PPh}_3$  to a  $\pi^*_{\text{NS}}$  orbital which is largely S in character.

An example of what has come to be recognized as a “typical” reaction for  $\text{Os}^{\text{VI}} \equiv \text{N}$  is shown in eq 16a (Scheme 8). In this case, triphenylphosphine undergoes a rapid reaction with  $\text{Os}^{\text{VI}} \equiv \text{N}$  to give the corresponding phosphoraninato product.<sup>56</sup> The kinetics are first order in each reagent with  $k(\text{CH}_3\text{CN}, 25.0^\circ\text{C}) = (1.36 \pm 0.08) \times 10^4 \text{ M}^{-1} \text{ s}^{-1}$  and no evidence for an intermediate. This reaction is analogous to

O-atom transfer from  $\text{cis-}[\text{Ru}^{\text{IV}}(\text{bpy})_2(\text{py})(\text{O})]^{2+}$  to triphenylphosphine, Table 1,<sup>27</sup> but with formal transfer of  $\text{N}^-$ . It probably occurs by initial electron pair donation from  $\text{PPh}_3$  to  $d\pi^*_1$  at  $\text{Os}^{\text{VI}} \equiv \text{N}$ , Figure 10A. Alternatively, it could occur by initial coordination expansion followed by intramolecular coupling (eq 16b, Scheme 8).

Reactions also occur with secondary amines such as morpholine and piperidine as shown in eq 17a (Scheme 8).<sup>57</sup> The proton in the initial adduct,  $\text{Os}^{\text{IV}}(\text{tpy})(\text{Cl})_2(\text{N}_\alpha\text{N}_\beta(\text{H})\text{R}_2)^+$ , is transferred to  $\text{N}_\alpha$ . It is acidic and easily deprotonated by a second base molecule, eq 17a. The net reaction is further complicated by a following electron transfer to a second  $\text{Os}^{\text{VI}} \equiv \text{N}^+$  to give  $\text{Os}^{\text{V}}-\text{NNR}_2^+$  and  $\text{Os}^{\text{V}} \equiv \text{N}$ . The latter couples to give the  $\mu\text{-N}_2$  dimer, eq 17b.<sup>57,58</sup> The initial reaction is first order in Os(VI) and second order in amine with  $k(\text{CH}_3\text{CN}, 25^\circ\text{C}) = (58.1 \pm 1.2) \text{ M}^{-2} \text{ s}^{-1}$  for  $\text{trans-}[\text{Os}^{\text{V}}(\text{tpy})(\text{Cl})_2(\text{NN}(\text{CH}_2)_4\text{O})]^+$  and  $k(\text{CH}_3\text{CN}, 25^\circ\text{C}) = 268 \pm 4.0 \text{ M}^{-2} \text{ s}^{-1}$  for  $\text{fac-}[\text{Os}^{\text{V}}(\text{tpm})(\text{Cl})_2(\text{NN}(\text{CH}_2)_4\text{O})]^+$ . A schematic orbital energy diagram for the  $\text{Os}^{\text{IV}}-\text{NNR}_2$  products is shown in Figure 10C. In this scheme, there are  $d\pi_{\text{Os}}$  interactions both with a  $p\pi$  orbital on  $\text{N}_\alpha$  and with the antibonding N–N orbital of  $\pi$  symmetry,  $\pi^*_{\text{N-N}}$ . This is the antibonding complement of  $\pi_{\text{N-N}}$ .

**8. Reactivity of Os Hydrazido Complexes: Electron Transfer and Proton-Coupled Electron Transfer.** The reactivity of the hydrazido complexes is also impressive. A cyclic voltammogram of  $\text{trans-}[\text{Os}^{\text{V}}(\text{tpy})(\text{Cl})_2(\text{NN}(\text{CH}_2)_4\text{O})]^+$  in 0.1 M  $\text{Bu}_4\text{NPF}_6/\text{CH}_3\text{CN}$ , Figure 11, reveals the existence of reversible couples at 0.98 V for Os(VI/V), at 0.00 V for Os(V/IV), and at  $-0.79$  V for Os(IV/III), versus SSCE.

Systematic changes occur in UV–visible spectra as the electron content changes and low-energy bands appear in the near-infrared. The spectral changes and the changes in

(53) Williams, D. S.; Meyer, T. J.; White, P. S. *J. Am. Chem. Soc.* **1995**, *117*, 823–824.

(54) El-Samanody, E. S.; Demadis, K. D.; Gallagher, L. A.; Meyer, T. J.; White, P. S. *Inorg. Chem.* **1999**, *38*, 3329–3336.

(55) Huynh, M. H. V.; White, P. S.; Meyer, T. J. *Inorg. Chem.* **2000**, *39*, 2825–2830.

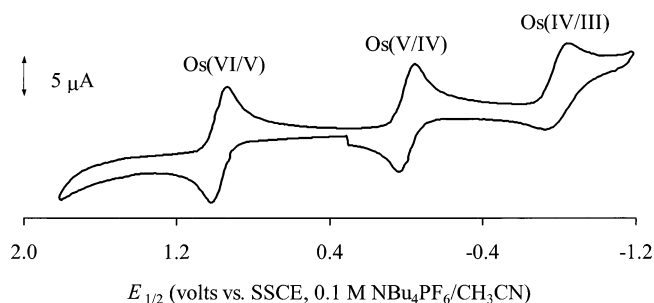
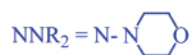
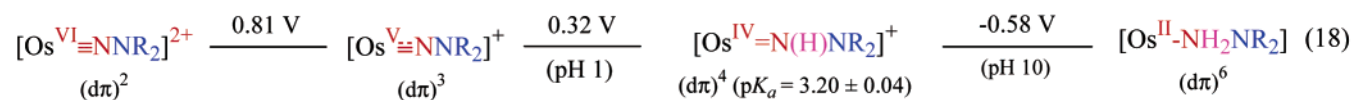
(56) (a) Bakir, M.; White, P. S.; Dovletoglou, A.; Meyer, T. J. *Inorg. Chem.* **1991**, *30*, 2835–2836. (b) Demadis, K. D.; Bakir, M.; Kleszczewski, B. G.; Williams, D. S.; White, P. S.; Meyer, T. J. *Inorg. Chim. Acta* **1998**, *270*, 511–526.

(57) Huynh, M. H. V.; El-Samanody, E.-S.; Demadis, K. D.; White, P. S.; Meyer, T. J. *J. Am. Chem. Soc.* **1999**, *121*, 1403–1404.

(58) Huynh, M. H. V.; El-Samanody, E.-S.; Demadis, K. D.; White, P. S.; Meyer, T. J. *Inorg. Chem.* **2000**, *39*, 3075–3085.

**Table 2.** Electron–Structure Correlations for Os(VI,V,IV)–Hydrazido Complexes (Os–N<sub>α</sub>N<sub>β</sub>R<sub>2</sub>) Taken from the Structures of *trans*-[Os<sup>VI</sup>(tpy)(Cl)<sub>2</sub>(NN(CH<sub>2</sub>)<sub>4</sub>O)]<sup>2+</sup>, *trans*-[Os<sup>V</sup>(tpy)(Cl)<sub>2</sub>(NN(CH<sub>2</sub>)<sub>4</sub>O)]<sup>+</sup>, and *cis*-[Os<sup>IV</sup>(tpy)(Cl)(NCCH<sub>3</sub>)(NN(CH<sub>2</sub>)<sub>4</sub>O)]<sup>+</sup><sup>a</sup>

	$\text{Os}^{\text{IV}}=\text{N}-\text{NR}_2$ <b>Os(IV)</b> <b>(d<sup>4</sup>)</b>	$\text{Os}^{\text{V}}\overset{\delta^+}{\equiv}\text{N}-\text{NR}_2$ <b>Os(V)</b> <b>(d<sup>3</sup>)</b>	$\text{Os}^{\text{VI}}\overset{+}{\equiv}\text{N}-\text{NR}_2$ <b>Os(VI)</b> <b>(d<sup>2</sup>)</b>
Os–N <sub>α</sub> (Å)	1.98	1.85	1.78
N <sub>α</sub> –N <sub>β</sub> (Å)	1.24	1.24	1.23
∠Os–N <sub>α</sub> –N <sub>β</sub> (°)	131	153	170
Electronic Configuration	dδ <sup>2</sup> dπ <sub>1</sub> * <sup>2</sup> dπ <sub>2</sub> * <sup>0</sup>	dδ <sup>2</sup> dπ <sub>1</sub> * <sup>1</sup>	dδ <sup>2</sup> dπ <sub>1</sub> * <sup>0</sup>

<sup>a</sup> The orbital ordering scheme is from Figure 10C.<sup>58</sup>**Scheme 9****Figure 11.** Cyclic voltammogram of *trans*-[Os<sup>V</sup>(tpy)(Cl)<sub>2</sub>(NN(CH<sub>2</sub>)<sub>4</sub>O)]-PF<sub>6</sub> in 0.2 M Bu<sub>4</sub>PF<sub>6</sub>/CH<sub>3</sub>CN at 25.0 °C, V versus SSCE.

structure are summarized in Table 2 for oxidation states VI, V, and IV. They can be accounted for by the schematic energy level diagram in Figure 10C.

As the electron content decreases from d<sup>4</sup> Os(IV) to d<sup>2</sup> Os(VI), the Os–N bond shortens from 1.98 to 1.78 Å. This is a consequence of a decrease in electron content in the antibonding dπ\*<sub>1</sub> orbital. The Os(IV) complexes are diamagnetic showing that the energy separation between dπ\*<sub>1</sub> and dπ\*<sub>2</sub> in Figure 10C is ≫k<sub>B</sub>T. On the basis of measurements in the near-infrared, the energies of the transitions dδ<sup>2</sup>dπ\*<sub>1</sub><sup>2</sup> → dδ<sup>2</sup>dπ\*<sub>1</sub><sup>1</sup>dπ\*<sub>2</sub><sup>1</sup> and dδ<sup>1</sup>dπ\*<sub>1</sub><sup>2</sup> → dδ<sup>1</sup>dπ\*<sub>1</sub><sup>1</sup>dπ\*<sub>2</sub><sup>1</sup> are 1.52 × 10<sup>4</sup> and 1.73 × 10<sup>4</sup> cm<sup>-1</sup>. From these values and assuming a constant pairing energy, the energy difference between dπ\*<sub>2</sub> and dπ\*<sub>1</sub> is 2.10 × 10<sup>3</sup> cm<sup>-1</sup>.<sup>58</sup>

The decrease in Os–N bond length is paralleled by an increase in the Os–N–N angle from 131° to 170°. The bending in Os(IV) decreases electron–electron repulsion. There is essentially no change in the N–N bond distance.

This is a remarkable example where the same overall bonding scheme persists through three oxidation states because the redox orbitals are largely dπ<sub>Os</sub> in character.<sup>59</sup>

A significant change occurs in the redox chemistry if water is added as a proton donor. This is illustrated by the redox potentials for couples based on *trans*-[Os<sup>V</sup>(tpy)(Cl)<sub>2</sub>(NNR<sub>2</sub>)]<sup>+</sup>, in 1:1 (v/v) H<sub>2</sub>O:CH<sub>3</sub>CN mixtures (μ = 1.0 M), in eq 18 (Scheme 9).

The potential for the Os(VI/V) couple is largely unaffected by added water, but reduction to Os(IV) results in protonation below pH 3.2. Further reduction gives an Os(II) hydrazine complex.<sup>57</sup> The change in proton content between Os(V) and Os(IV) is reminiscent of the Ru<sup>IV</sup>=O<sup>2+</sup>/Ru<sup>III</sup>–OH<sup>2+</sup> couple for *cis*-[Ru<sup>IV</sup>(bpy)<sub>2</sub>(py)(O)]<sup>2+</sup>. This observation raised the interesting possibility that proton-coupled electron transfer might play an important mechanistic role for this couple as well.

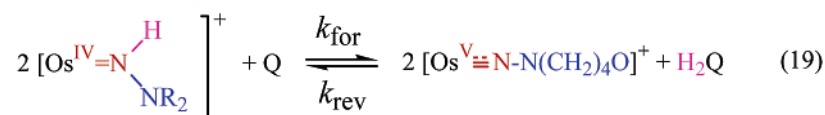
We explored this possibility by studying the oxidation of *trans*-[Os<sup>IV</sup>(tpy)(Cl)<sub>2</sub>(N(H)N(CH<sub>2</sub>)<sub>4</sub>O)]<sup>+</sup> (Os<sup>IV</sup>–N(H)N(CH<sub>2</sub>)<sub>4</sub>–O<sup>+</sup>) to *trans*-[Os<sup>V</sup>(tpy)(Cl)<sub>2</sub>(NN(CH<sub>2</sub>)<sub>4</sub>O)]<sup>+</sup> (Os<sup>V</sup>–NN(CH<sub>2</sub>)<sub>4</sub>–O<sup>+</sup>) by quinone (Q) to give H<sub>2</sub>Q. The net reaction is shown in eq 19 (Scheme 10).<sup>60a</sup> Since it occurs with ΔG° = –0.045 eV, it is possible to study the kinetics in both the forward and reverse directions.

As shown by the rate laws in eq 20 (Scheme 11), the reaction in the forward direction is first order in Q and first order in Os<sup>IV</sup>=N(H)N(CH<sub>2</sub>)<sub>4</sub>O<sup>+</sup>. The reverse reaction is more complex with Os<sup>V</sup>–NN(CH<sub>2</sub>)<sub>4</sub>O<sup>+</sup> appearing to second order.<sup>60b</sup>

Kinetic studies in the forward direction reveal the existence of parallel pathways. One is pH dependent, and the other is

(59) Huynh, M. H. V.; El-Samanody, E.-S.; White, P. S.; Meyer, T. J. *Inorg. Chem.* **1999**, *38*, 3760–3761.(60) (a) Huynh, M. H. V.; White, P. S.; Meyer, T. J. *J. Am. Chem. Soc.* **1999**, *121*, 4530–4531. (b) Huynh, M. H. V.; Meyer, T. J. Manuscript in preparation. The kinetic isotope effect of 439 ± 6 reported here rather than of 41 ± 1 is correct. In the earlier work, the kinetic analysis failed to account properly for the pH dependence, see ref 61b.

Scheme 10

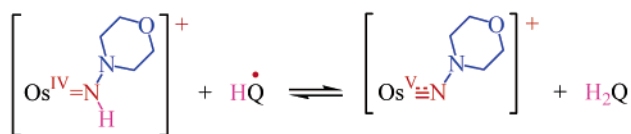
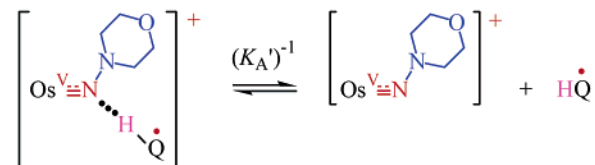
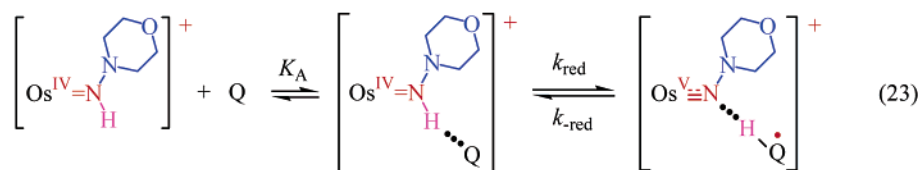
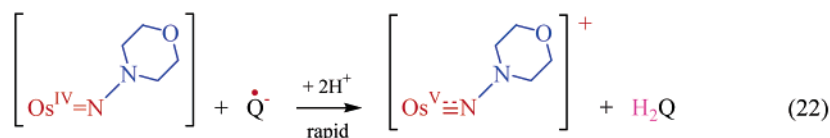
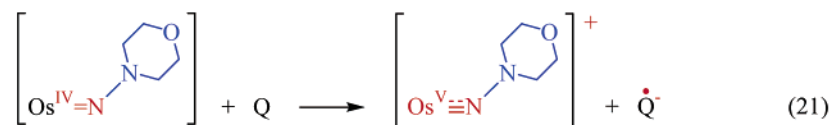


Scheme 11

$$\text{Forward:} \quad \frac{-d[\text{Os}(\text{IV})]}{dt} = k_{\text{for}} [\text{Q}][\text{Os}(\text{IV})] \quad (20)$$

$$\text{Reverse:} \quad \frac{-d[\text{Os}(\text{V})]}{dt} = k_{\text{rev}} \frac{[\text{Os}^{\text{V}}\equiv\text{N}(\text{CH}_2)_4\text{O}^+]^2 [\text{H}_2\text{Q}]}{[\text{Os}^{\text{IV}}=\text{N}(\text{H})\text{N}(\text{CH}_2)_4\text{O}^+]}$$

Scheme 12



pH independent. In the pH-dependent pathway, initial deprotonation of  $\text{Os}^{\text{IV}}=\text{N}(\text{H})\text{N}(\text{CH}_2)_4\text{O}^+$  occurs to give  $\text{Os}^{\text{IV}}=\text{NN}(\text{CH}_2)_4\text{O}$ . It undergoes outer-sphere electron transfer to Q to give  $\text{Os}^{\text{V}}\equiv\text{NN}(\text{CH}_2)_4\text{O}^+$  and  $\text{Q}^{\bullet-}$ , eq 21 (Scheme 12). This step is followed by rapid electron/proton transfer steps to give the final products, eq 22 (Scheme 12).

The acid-independent pathway is far more interesting. It occurs by the mechanism shown in eq 23 (Scheme 12). In the initial step, there is a preassociation to form what is probably a hydrogen-bonded adduct between protonated  $\text{Os}^{\text{IV}}=\text{N}(\text{H})\text{N}(\text{CH}_2)_4\text{O}^+$  and Q. It is observed spectroscopically at high concentrations of Q as is the reverse intermediate which is an adduct between  $\text{Os}^{\text{V}}\equiv\text{NN}(\text{CH}_2)_4\text{O}^+$  and  $\text{HQ}^{\bullet}$ . The intermediates also reveal themselves in the appearance

of saturation kinetics in [Q] in the forward direction and in  $[\text{H}_2\text{Q}]$  in the reverse direction. This allows the kinetically observed rate constants to be factored into the preassociation constants,  $K_A$  or  $K_A'$  and  $k_{\text{red}}$  or  $k_{-\text{red}}$ .

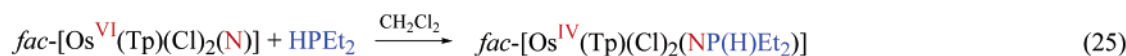
When the kinetics were studied in 1:1 (v/v)  $\text{D}_2\text{O}:\text{CH}_3\text{CN}$  mixtures and compared to 1:1 (v/v)  $\text{H}_2\text{O}:\text{CH}_3\text{CN}$ , the colossal  $\text{H}_2\text{O}/\text{D}_2\text{O}$  kinetic isotope effect (KIE) of  $439 \pm 6$  was observed for the redox step, Table 3. On the basis of the results of a mole fraction study in  $\text{H}_2\text{O}/\text{D}_2\text{O}$  mixtures, only a single proton is involved in the redox step.

In the initial report of this reaction, the  $\text{H}_2\text{O}/\text{D}_2\text{O}$  kinetic isotope effect was reported to be 41.<sup>53a</sup> This value is a lower limit because the influence of the pH-dependent pathway was not properly taken into account as was done, for

**Table 3.** Kinetic Isotope Effects at  $25.0 \pm 0.1$  °C in 1:1 (v/v)  $\text{CH}_3\text{CN}:\text{H}_2\text{O}$  for Proton-Coupled Electron Transfer Based on O, S, N, and P Donor Atoms

Reactions (in 1:1 (v/v) $\text{CH}_3\text{CN}:\text{H}_2\text{O}$ )	$k_{\text{red}}^{\text{H}_2\text{O}} / k_{\text{red}}^{\text{D}_2\text{O}}$	$K_{\text{A}}^{\text{H}_2\text{O}} / K_{\text{A}}^{\text{D}_2\text{O}}$
$\text{Cis-}[\text{Ru}^{\text{IV}}(\text{bpy})_2(\text{py})(\text{O})]^{2+} + \text{H}_2\text{Q}$	$(k_{\text{red}}K_{\text{A}})$ $30 \pm 1^{\text{a}}$	N/A
$\text{Trans-}[\text{Os}^{\text{IV}}(\text{tpy})(\text{Cl})_2(\text{NS}(\text{H})\text{C}_6\text{H}_4\text{Me})]^{+} + \text{Q}$	$189 \pm 5$	$1.05 \pm 0.02$
$\text{Trans-}[\text{Os}^{\text{IV}}(\text{tpy})(\text{Cl})_2(\text{N}(\text{H})\text{N}(\text{CH}_2)_4\text{O})]^{+} + \text{Q}$	$439 \pm 6$	$1.04 \pm 0.03$
$\text{Fac-}[\text{Os}^{\text{IV}}(\text{Tp})(\text{Cl})_2(\text{NP}(\text{H})\text{Et}_2)] + \text{Q}$	$175 \pm 5$	$1.02 \pm 0.02$

<sup>a</sup> In  $\text{H}_2\text{O}$  (pH = 4.45,  $\mu$  = 0.1 M, and  $T$  =  $20.0 \pm 0.2$  °C), the kinetic isotope effect is for the product  $k_{\text{red}}K_{\text{A}}$ .

**Scheme 13**

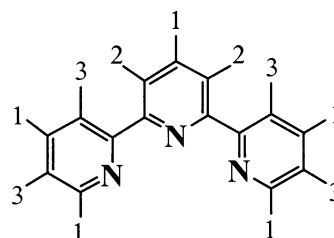
example, for the oxidation of  $\text{fac-}[\text{Os}^{\text{IV}}(\text{Tp})(\text{Cl})_2(\text{NPHEt}_2)]$  by Q, see below.<sup>61b</sup>

The generic  $\text{N}^-$  transfer reaction between  $\text{Os}^{\text{VI}}\equiv\text{N}$  and nucleophiles alluded to above includes reactions between  $\text{trans-}[\text{Os}^{\text{VI}}(\text{tpy})(\text{Cl})_2(\text{N})]^{+}$  and aromatic thiols, eq 24,<sup>61a</sup> and between  $\text{fac-}[\text{Os}^{\text{VI}}(\text{Tp})(\text{Cl})_2(\text{N})]$  and the secondary phosphine in eq 25 (Scheme 13).<sup>61b</sup>

The thermodynamic redox and acid–base properties of these two adducts are accidentally nearly comparable to those of the hydrazido complex. In both cases, the  $\text{p}K_{\text{A}}$  for  $\text{Os}(\text{IV})$  is between 3 and 5, and reactions with Q to give  $\text{H}_2\text{Q}$  occur with  $\Delta G^\circ \sim 0$  eV. The reactions with Q are pH-dependent. Spectroscopically observable intermediates can be detected, and saturation kinetics appear for the acid-independent pathway. Detailed kinetic analyses of the three systems have yielded the  $\text{H}_2\text{O}:\text{D}_2\text{O}$  kinetic isotope effects listed in Table 3.

These data are remarkable for demonstrating the existence of colossal kinetic isotope effects for proton-coupled electron transfer. Alternate pathways involving sequential rather than concerted electron–proton transfer exist, but they involve unstable intermediates and high reaction barriers and are uncompetitive. The mechanisms that dominate involve simultaneous electron–proton transfer and proton tunneling from levels well below the intersection between potential curves as illustrated in Figure 2.

**9. Reactions at 2,2':6',2''-Terpyridine.** There is another remarkable aspect of the reactivity of hydrazido complexes which is tied to multiple oxidation states but based on the tpy ligand in  $\text{trans-}[\text{Os}^{\text{VI}}(\text{tpy})(\text{Cl})_2(\text{NN}(\text{CH}_2)_4\text{O})]^{2+}$ . In this complex, the C–H protons of the terpyridyl ligand undergo relatively rapid exchange with  $\text{D}_2\text{O}$  in  $\text{D}_2\text{O}:\text{CH}_3\text{CN}$  mixtures at pH 7 as shown by  $^1\text{H}$  NMR measurements.<sup>62a</sup> Referring to the labeling pattern in Chart 1, the rate of C–H/C–D exchange by position on the tpy rings falls in the order

**Chart 1**

$1 > 2 > 3$ . This demonstrates a selective activation of the C–H terpyridyl bonds to H–D exchange by the  $\text{Os}(\text{VI})$  “substituent”.

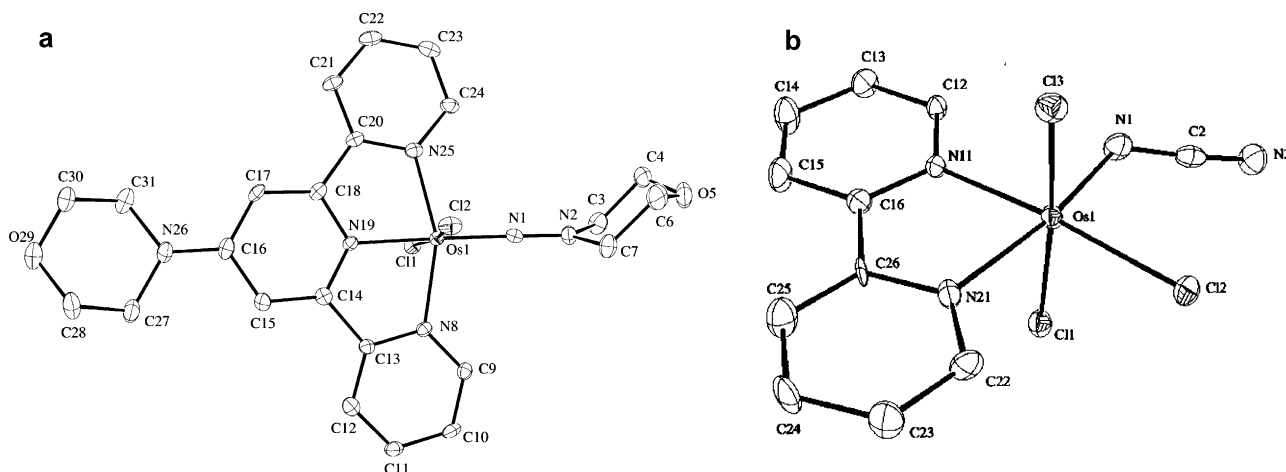
The unusual ligand reactivity in these high oxidation state complexes extends to nucleophilic additions at the central pyridyl ring. These reactions are facile at room temperature. The nucleophiles include a range of N and O bases. The net reaction with morpholine is shown in eq 26 (Scheme 14) and the structure of the  $\text{Os}(\text{VI})$  product in Figure 12A.<sup>62b</sup> A kinetic study has revealed a rate law first order in unsubstituted  $\text{Os}^{\text{VI}}\equiv\text{NN}(\text{CH}_2)_4\text{O}^{2+}$  and second order in morpholine. The mechanism appears to involve nucleophilic attack of morpholine at the 1-position of the central tpy ring in  $\text{trans-}[\text{Os}^{\text{VI}}(\text{tpy})(\text{Cl})_2(\text{NN}(\text{CH}_2)_4\text{O})]^{2+}$  accompanied by internal  $2e^-$  reduction of the morpholine complex to give tpy-substituted  $\text{Os}(\text{IV})$ . Once formed, it undergoes electron transfer with two unreacted  $\text{Os}^{\text{VI}}\text{-NN}(\text{CH}_2)_4\text{O}^{2+}$  molecules to give the final mix of products shown in eq 26.

**10. Additional Reactions of  $\text{Os}(\text{VI})$  Nitrido Complexes and Their  $\text{Os}(\text{IV})$  Adducts.** The two-electron,  $\text{N}^-$ -transfer chemistry between  $\text{Os}^{\text{VI}}\equiv\text{N}$  and nucleophiles extends to a variety of bases. Continuing studies are revealing that the  $\text{Os}^{\text{IV}}\equiv\text{NNR}_2$ ,  $\text{Os}^{\text{IV}}\equiv\text{NSAr}$ , and  $\text{Os}^{\text{IV}}\text{-NPR}_3$  adducts are all redox active. In fact, the scope of their redox reactivities can far exceed those of the  $\text{Os}^{\text{VI}}\equiv\text{N}$  precursor.

(61) (a) Huynh, M. H. V.; White, P. S.; Meyer, T. J. *Angew. Chem., Int. Ed.* **2000**, *39* (22), 4101–4104. (b) Huynh, M. H. V.; Meyer, T. J. *Angew. Chem., Int. Ed.* **2002**, *41* (8), 1395–1398.

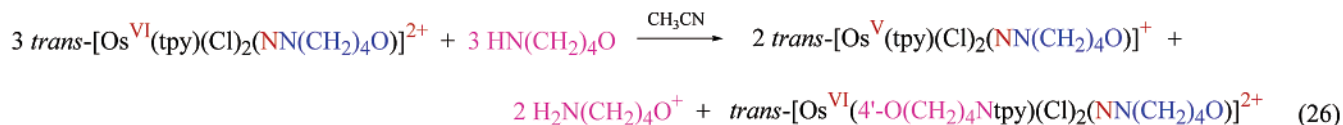
(62) (a) Huynh, M. H. V.; Lee, D. G.; White, P. S.; Meyer, T. J. *J. Am. Chem. Soc.* **1999**, *121*, 10446–10447. (b) Huynh, M. H. V.; Lee, D. G.; White, P. S.; Meyer, T. J. *Inorg. Chem.* **2001**, *40*, 3842–3849.



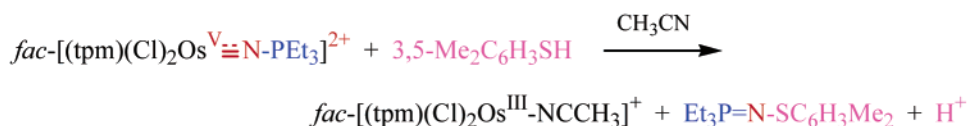
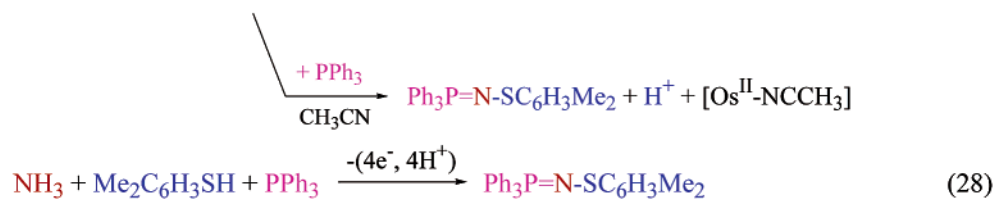
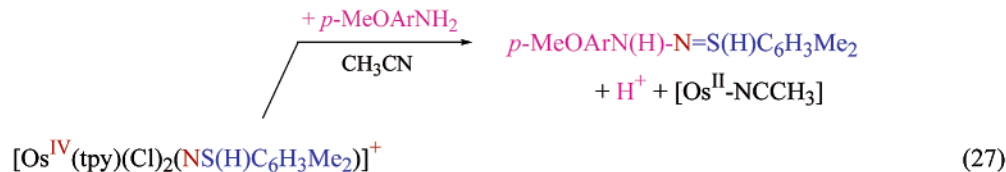


**Figure 12.** (A) ORTEP diagram (30% ellipsoids) and labeling scheme for the cation in  $trans\text{-}[\text{Os}^{\text{VI}}(4'\text{-O}(\text{CH}_2)_4\text{Ntpy})(\text{Cl})_2(\text{NN}(\text{CH}_2)_4\text{O})](\text{PF}_6)_2$ . (B) ORTEP diagram (30% ellipsoids) and labeling scheme for  $[\text{Os}^{\text{IV}}(\text{bpy})(\text{Cl})_3(\text{NCN})]^-$ .

#### Scheme 14



#### Scheme 15



It is possible to anticipate this reactivity based on the energy level diagram in Figure 10C for  $\text{Os}^{\text{IV}}=\text{NNR}_2$ . Reactivity as an oxidant is expected, analogous to oxo complexes, based on electron donation to the empty  $d\tau_2^*$  orbital which is antibonding and largely Os in character. Rehybridization at  $\text{N}_\alpha$  with loss of the N–N multiple bond interaction and the assumption of  $\text{sp}^2$  character provides an orbital basis for  $\sigma$ -bond formation at  $\text{N}_\alpha$ .

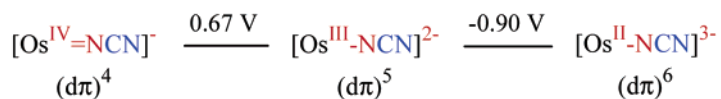
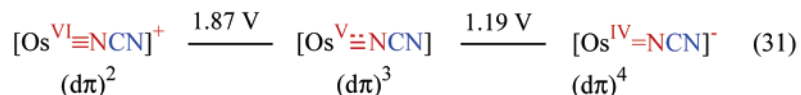
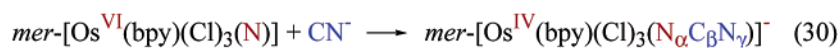
Two reactions of this kind are illustrated in eq 27 (Scheme 15) in which either  $p\text{-MeOC}_6\text{H}_4\text{NH}_2$  or  $\text{PPh}_3$  is added to  $trans\text{-}[\text{Os}^{\text{IV}}(\text{tpy})(\text{Cl})_2(\text{NS}(\text{H})\text{C}_6\text{H}_3\text{Me}_2)]^+$ .<sup>63</sup> The solvento complex,  $trans\text{-}[\text{Os}^{\text{III}}(\text{tpy})(\text{Cl})_2(\text{NCCH}_3)]^+$ , and the organic heteroatom compounds,  $p\text{-MeOC}_6\text{H}_4\text{N}(\text{H})\text{N}=\text{S}(\text{H})\text{C}_6\text{H}_3\text{Me}_2$  or  $\text{Ph}_3\text{P}=\text{N-SC}_6\text{H}_3\text{Me}_2$ , are the final products. The aminosulfur-

imine and phosphinosulfimine adducts are initially formed in the coordination sphere. They are subsequently released by solvolysis to give the final organic products and  $trans\text{-}[\text{Os}^{\text{II}}(\text{tpy})(\text{Cl})_2(\text{NCCH}_3)]$ .

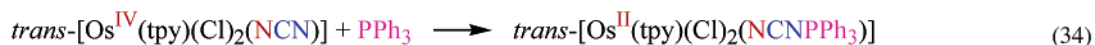
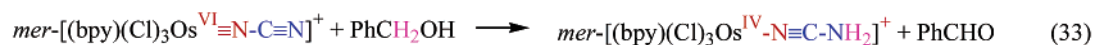
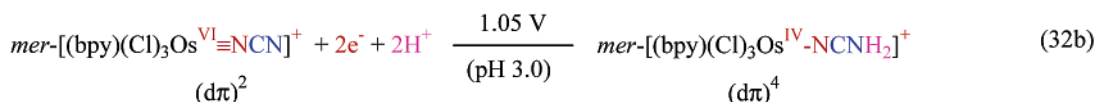
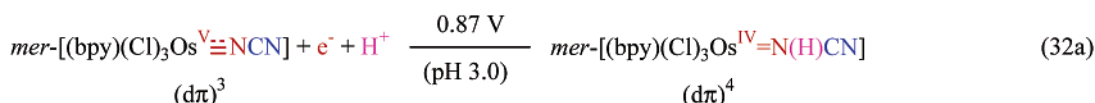
Addition of the second nucleophile to Os(IV) leads to a significant change in electronic structure at the metal with loss of Os–N multiple bonding accompanying formation of Os(II). The sulfur-derivatized phosphoraniminato organic product can be viewed as an analogue of triphenylphosphine oxide.

(63) (a) Huynh, M. H. V.; Jameson, D. L.; Meyer, T. J. *Inorg. Chem.* **2001**, *40*, 5062–5063. (b) Huynh, M. H. V.; El-Samanody, E.-S.; Demadis, K. D.; White, P. S.; Meyer, T. J. Manuscript in preparation.

Scheme 16



Scheme 17



The reactions in eq 27 are notable in (1) illustrating sequential two-electron-transfer reactions analogous to those observed for the Ru(VI)–dioxo complex in eq 7 but based on a single N atom, (2) revealing the transfer of large organic fragments from Os(IV) in reactions analogous to  $\text{N}^-$  transfer, and (3) using  $\text{N}^-$  transfer followed by  $\text{NS}(\text{H})\text{C}_6\text{H}_3\text{Me}_2^-$  group transfer as a general synthetic route for the double derivatization of N and a new route to N-based heteroatom compounds. For the triphenylphosphine example in eq 27, the net reaction beginning with the preparation of the nitrido complex, by reaction between  $\text{Os}^{\text{VIII}}\text{O}_4$  and  $\text{NH}_3$  in the presence of tpy and  $\text{Cl}^-$ , is given by eq 28 (Scheme 15).

The tris(pyrazolyl)methane complex  $\text{fac-}[\text{Os}^{\text{IV}}(\text{tpm})(\text{Cl})_2(\text{NPET}_3)]^+$  is more electron rich than the tpy complex. Reactions with a second nucleophile are far slower than for the tpy complex. A second addition to N can be induced in this case by oxidation to Os(V). It undergoes a rapid reaction with 3,5-dimethylbenzenethiol, eq 29 (Scheme 15).<sup>63</sup>

The reaction between nucleophiles and  $\text{Os}^{\text{VI}}\equiv\text{N}$  is quite general. The reaction between  $\text{CN}^-$  and  $\text{mer-}[\text{Os}^{\text{VI}}(\text{bpy})(\text{Cl})_3(\text{N})]$  is shown in eq 30 (Scheme 16),<sup>64a</sup> and the crystal structure of the Os(IV)–cyanoimido adduct in Figure 12B. Features in this structure, consistent with the generic energy level diagram in Table 2, are the Os–N bond length of 1.914 Å and the Os–N–C bond angle of 131°.

The redox reactivity of the Os(IV)–cyanoimido product is like that of the hydrazido complexes described earlier but with some new wrinkles. In cyclic voltammograms in dry  $\text{CH}_3\text{CN}$ , chemically reversible waves appear for couples ranging from Os(VI/V) at 1.87 V to Os(III/II) at –0.90 V, eq 31 (0.2 M  $\text{Bu}_4\text{NPF}_6/\text{CH}_3\text{CN}$ , V versus SSCE) (Scheme 16).

As in the oxo/hydroxo/aqua cases cited earlier, there is a pH-dependence in the lower oxidation state couples with added water. From pH-dependent electrochemical studies, the Os(V/IV) and Os(VI/IV) couples involve the addition of electrons and protons as shown in eq 32 (Scheme 17) in 1:1 (v/v)  $\text{CH}_3\text{CN}:\text{H}_2\text{O}$  at pH = 3.0.<sup>64b</sup> IR studies clearly delineate that addition of a single proton occurs at  $\text{N}_\alpha$  and addition of two protons at  $\text{N}_\beta$ .

The similarity in pH-dependence extends to an oxo/nitrido-like reactivity in the higher oxidation states. Benzyl alcohol is oxidized to benzaldehyde by  $\text{Os}^{\text{VI}}\equiv\text{N}-\text{C}\equiv\text{N}^+$ , eq 33 (Scheme 17), by a reaction first order in both Os(VI) and the alcohol with  $k_{\text{obs}}(\text{CH}_3\text{CN}, 25.0 \pm 0.1 \text{ }^\circ\text{C}) = (8.6 \pm 0.2) \times 10^2 \text{ M}^{-1} \text{ s}^{-1}$ . In this reaction, net transfer of  $2\text{e}^-$  and  $2\text{H}^+$  occurs from the alcohol to  $\text{Os}^{\text{VI}}\equiv\text{N}-\text{C}\equiv\text{N}^+$ .<sup>64b</sup>

The  $\text{NCN}^{2-}$  ligand is also capable of supporting  $\text{NCN}^0$  transfer from Os(IV), analogous to  $\text{N}^-$  transfer from  $\text{Os}^{\text{VI}}\equiv\text{N}$  as shown by the reaction with  $\text{PPh}_3$  in eq 34 (Scheme 17). In this case, the N(cyano)iminophosphorane product, which is a phosphine oxide analogue, remains coordinated in the Os(II) product. Binding at  $\text{N}_\gamma$  has been confirmed by IR.<sup>64b</sup>

As summarized in eq 35 (Scheme 18), there is also an extensive acid–base chemistry at the  $\text{NCN}^{2-}$  ligand bound to Os(IV).<sup>64a</sup> As noted above, monoprotonation occurs at  $\text{N}_\alpha$ . Addition of a second proton occurs at  $\text{N}_\gamma$  concomitantly with transfer of the first proton from  $\text{N}_\alpha$  to  $\text{N}_\gamma$ . The terminal  $\text{N}_\gamma$  atom is also reactive as a nucleophile toward both alkylation and acylation.

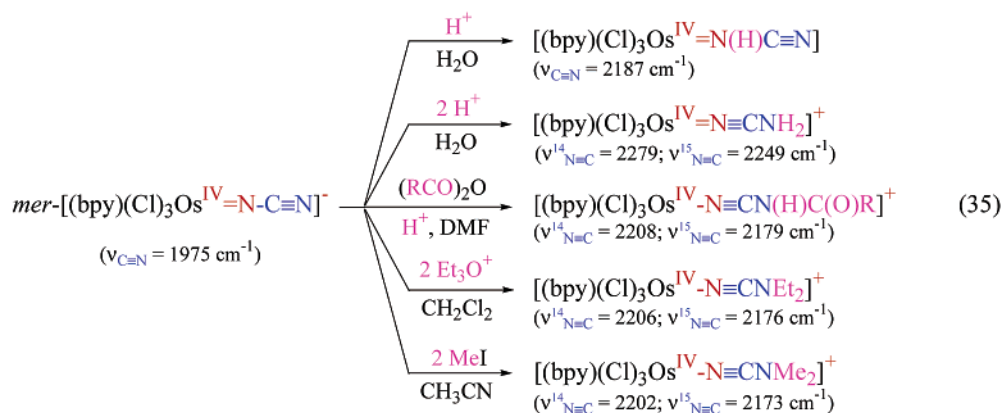
There is also an as yet unpublished reactivity chemistry with thiocyanate ( $\text{NCS}^-$ ) to give  $\text{trans-}[\text{Os}^{\text{IV}}(\text{tpy})(\text{Cl})_2(\text{NSCN})]$  and with cyanate ( $\text{OCN}^-$ ) to give  $\text{trans-}[\text{Os}^{\text{IV}}(\text{tpy})(\text{Cl})_2(\text{NOCN})]$ .<sup>65</sup>

A novel case that was recently published is the reaction with  $\text{N}_3^-$  shown in eq 36 (Scheme 19).<sup>66</sup> The product of

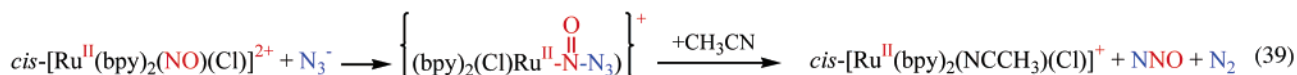
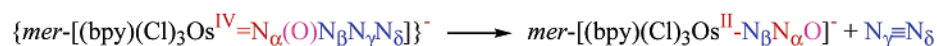
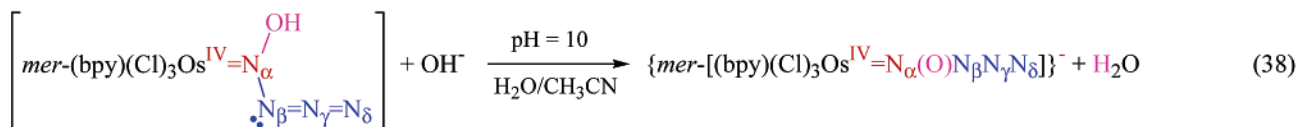
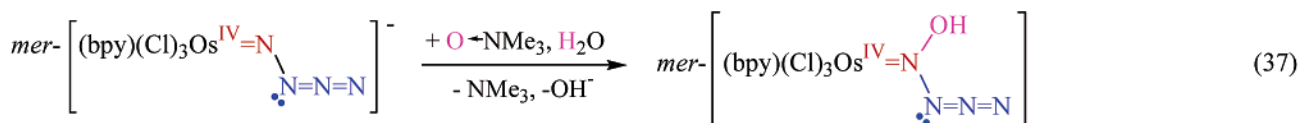
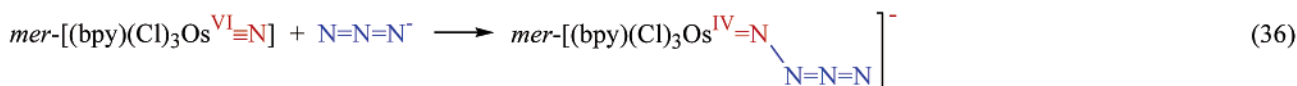
(64) (a) Huynh, M. H. V.; White, P. S.; Carter, C. A. G.; Meyer, T. J. *Angew. Chem., Int. Ed.* **2001**, *40* (16), 3037–3039. (b) Huynh, M. H. V.; Meyer, T. J.; Baker, R. T. *J. Am. Chem. Soc.* **2003**, *125*, 2832–2833.

(65) Huynh, M. H. V.; Meyer, T. J. Work in progress.

Scheme 18



Scheme 19



this reaction,  $\text{mer}-[\text{Os}^{\text{IV}}(\text{bpy})(\text{Cl})_3(\text{N}_4)]^-$ , is the first example of the terminal  $\text{N}_4^{2-}$  ligand. There is an earlier example of  $\text{N}_4$  as a bridging ligand.<sup>67</sup> Although a crystal structure is not yet available, a combination of  $^{15}\text{N}$  NMR and IR measurements on  $^{15}\text{N}$ -labeled samples have been used to confirm the structure implied in eq 36.

The  $\text{Os}^{\text{IV}}$ -azidoimido complex has a fascinating reactivity chemistry of its own. An example is the net hydroxylation reaction in eq 37 (Scheme 19) in which the azidoimido ligand is converted into the azidohydroxoamido ( $\text{N}(\text{OH})\text{N}_3^-$ ) ligand. This is also the first example of this ligand. The complex was characterized by elemental analysis and IR with  $^{15}\text{N}$  labeling. It is unstable in basic solution. As shown in eq 38 (Scheme 19), loss of the hydroxyl proton gives the coordinated azidoamido dianion ( $\text{N}(\text{O})\text{N}_3^{2-}$ ). It is apparently unstable with regard to intramolecular electron transfer, extrusion of  $\text{N}_2$ , and formation of the  $\text{N}_2\text{O}$  complex,  $\text{mer}-[\text{Os}^{\text{II}}(\text{bpy})(\text{Cl})_3(\text{N}_2\text{O})]^-$ .

The  $\text{Os}^{\text{II}}-\text{N}_2\text{O}$  product is one of two characterized examples of coordinated dinitrogen oxide.<sup>68</sup> Analogues of the  $\text{N}(\text{O})\text{N}_3^{2-}$  intermediate have been invoked as transients

in the reactions between Ru-nitrosyl complexes and azide ion, eq 39 (Scheme 19).<sup>69</sup>

The results of  $^{15}\text{N}$ -labeling experiments have revealed an interesting twist in the formation of the  $\text{N}_2\text{O}$  product. They show that extrusion of  $\text{N}_2$  is accompanied by rotation of the ligand with the original N atom  $\alpha$  to Os shifted to the  $\beta$ -position in the  $\text{N}_2\text{O}$  product, eq 38.

**11. Ligand-Based Redox Chemistry.** Electronic interactions between osmium and the coordinated ligands in the  $\text{Os}^{\text{IV}}$  adducts open up new reactivity channels based on the ligands rather than the metal. A striking example is the O-atom transfer ability of *cis*- and *trans*- $[\text{Os}^{\text{IV}}(\text{tpy})(\text{Cl})_2(\text{NS}(\text{O})\text{C}_6\text{H}_3\text{Me}_2)]$  ( $\text{Os}^{\text{IV}}-\text{NS}(\text{O})\text{C}_6\text{H}_3\text{Me}_2$ ). The sulfoximido complexes are formed by O-atom transfer from  $\text{O}^-\text{NMe}_3$  to the corresponding *cis*- and *trans*- $[\text{Os}^{\text{IV}}(\text{tpy})(\text{Cl})_2(\text{NS}(\text{H})\text{C}_6\text{H}_3\text{Me}_2)]^+$  precursors, eq 40 (Scheme 20).<sup>70</sup> The O-atom transfer reactivity includes O-atom transfer to  $\text{PPh}_3$ , eq 41, and epoxidation of olefins, eq 42 (Scheme 20).

(66) Huynh, M. H. V.; Baker, R. T.; Jameson, D. L.; Labouriau, A.; Meyer, T. J. *J. Am. Chem. Soc.* **2002**, *124*, 4580–4582.

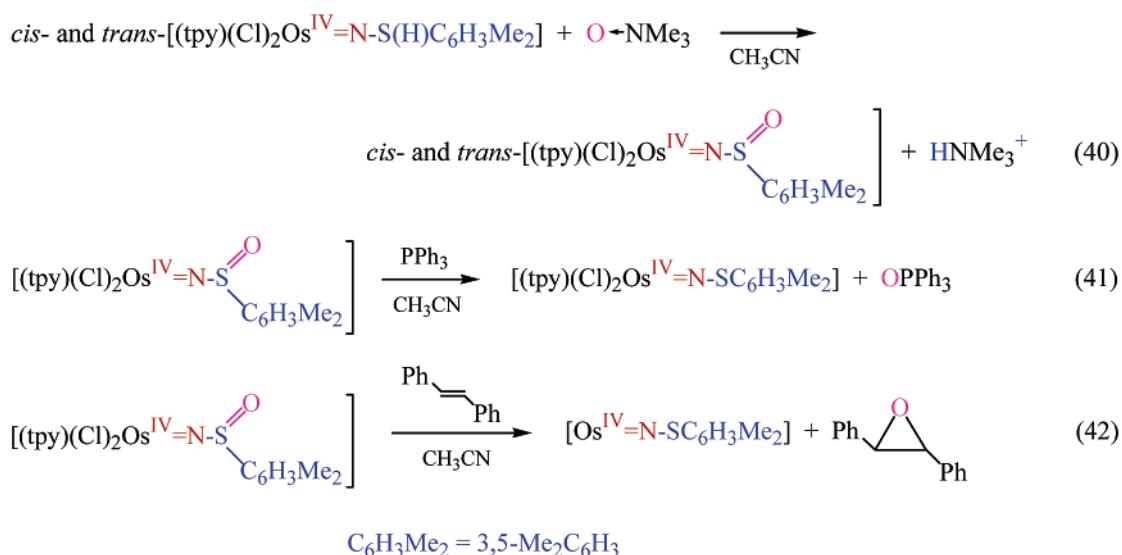
(67) Massa, W.; Kujanek, R.; Baum, G.; Dehnicke, K. *Angew. Chem., Int. Ed.* **1984**, *23* (2), 149.

(68) (a) Armor, J. N.; Taube, H. *J. Am. Chem. Soc.* **1970**, *92*, 2560–2562. (b) Armor, J. N.; Taube, H. *J. Am. Chem. Soc.* **1969**, *91*, 6874–6876.

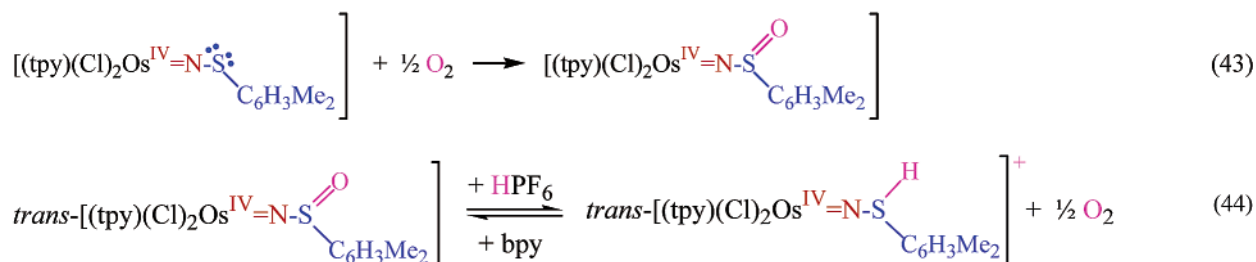
(69) (a) Miller, F. J.; Meyer, T. J. *J. Am. Chem. Soc.* **1971**, *93*, 1294. (b) Callahan, R. W.; Meyer, T. J. *Inorg. Chem.* **1977**, *16*, 574–581. (c) Bottomley, F.; Mukaida, M. *J. Chem. Soc., Dalton Trans.* **1982**, *10*, 1933–1937.

(70) Huynh, M. H. V.; White, P. S.; Meyer, T. J. *J. Am. Chem. Soc.* **2001**, *123*, 9170–9171.

## Scheme 20



## Scheme 21

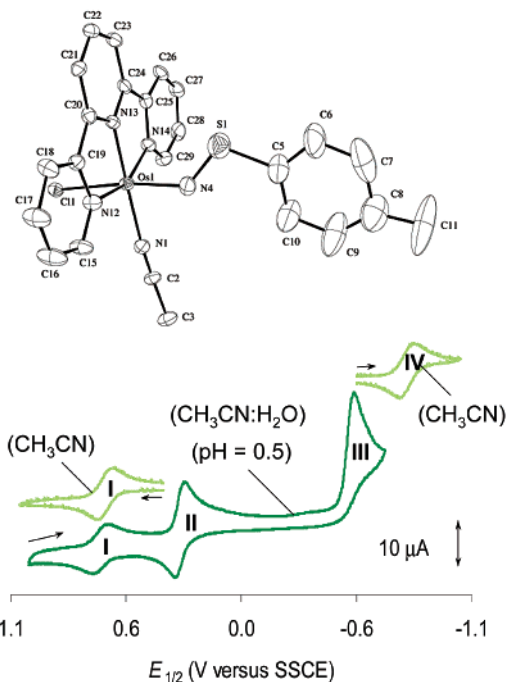


These reactions illustrate that facile oxygen-atom transfer can occur from the sulfoximido ligand bound to Os(IV). Electronic coupling between the sulfoximido ligand and Os(IV) is important. The ligand is highly activated toward atom transfer in the coordination sphere.

The deprotonated form,  $\text{trans-}[\text{Os}^{\text{IV}}(\text{tpy})(\text{Cl})_2(\text{NSC}_6\text{H}_3\text{Me}_2)]$ , undergoes rapid oxidation by  $\text{O}_2$  to give the sulfoximido form,  $\text{trans-}[\text{Os}^{\text{IV}}(\text{tpy})(\text{Cl})_2(\text{NS}(\text{O})\text{C}_6\text{H}_3\text{Me}_2)]$  ( $\text{Os}^{\text{IV}}-\text{NS}(\text{O})\text{C}_6\text{H}_3\text{Me}_2$ ), eq 43 (Scheme 21).<sup>70</sup> The combination of reactions in eqs 41–43 opens the possibility of creating  $\text{O}_2$ -based catalytic oxidation cycles, and this area is in need of further investigation.

Remarkably, the reactivity of the oxygen atom in  $\text{Os}^{\text{IV}}-\text{NS}(\text{O})\text{C}_6\text{H}_3\text{Me}_2$  also extends to the evolution of oxygen. Addition of stoichiometric  $\text{HPF}_6$  in  $\text{CH}_3\text{CN}$  results in the evolution of  $\text{O}_2$ , eq 44 (Scheme 21).<sup>71</sup> This reaction can be reversed by addition of sufficient 2,2'-bipyridine to deprotonate  $\text{Os}^{\text{IV}}-\text{NS}(\text{H})\text{C}_6\text{H}_3\text{Me}_2$ , eq 44. We have not been able to study the kinetics of these reactions because they are too rapid even at low temperatures with stopped-flow kinetics techniques.

There is another reaction of a coordinated ligand that may open new possibilities for chemical reactivity studies. The cyclic voltammogram of  $\text{cis-}[\text{Os}^{\text{IV}}(\text{tpy})(\text{Cl})(\text{NCCH}_3)(\text{NSC}_6\text{H}_4\text{Me})]^+$  ( $\text{C}_6\text{H}_4\text{Me} = 4\text{-MeC}_6\text{H}_4$ ) in  $\text{CH}_3\text{CN}$  displays an Os(V/IV) wave at  $E_{1/2} = 1.56$  V, an Os(IV/III) wave at  $E_{1/2} = 0.65$  V, and an Os(III/II) wave at  $E_{1/2} = -0.79$  V, Figure 13.<sup>72</sup>



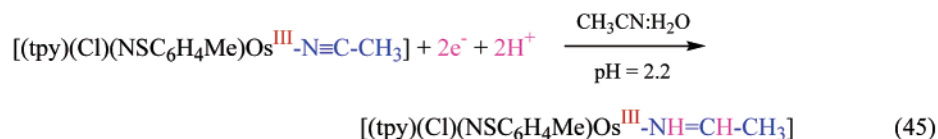
**Figure 13.** Cyclic voltammogram of  $\text{cis-}[\text{Os}^{\text{IV}}(\text{tpy})(\text{Cl})(\text{NCCH}_3)(\text{NSC}_6\text{H}_3\text{Me}_2)]^+$  in 1:1 (v/v)  $\text{CH}_3\text{CN}:\text{H}_2\text{O}$  at  $\text{pH} = 0.5$  and  $\mu = 1.0$  M in  $\text{NH}_4\text{PF}_6$  (waves I, II, and III) and in 0.2 M  $\text{CH}_3\text{CN}/\text{NH}_4\text{PF}_6$  (waves I and IV) (V versus SSCE). An ORTEP diagram (30% ellipsoids) and labeling scheme for  $\text{cis-}[\text{Os}^{\text{IV}}(\text{tpy})(\text{Cl})(\text{NCCH}_3)(\text{NSC}_6\text{H}_3\text{Me}_2)]^+$  is also shown.

(71) Huynh, M. H. V.; White, P. S.; Morris, D. E.; and Meyer, T. J. *Angew. Chem., Int. Ed.* **2002**, *41* (13), 2330–2333.

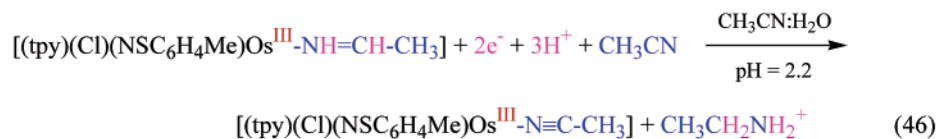
(72) Huynh, M. H. V.; White, P. S.; Meyer, T. J. *Angew. Chem., Int. Ed.* **2002**, *41* (20), 3870–3873.

## Scheme 22

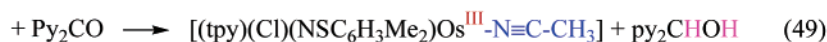
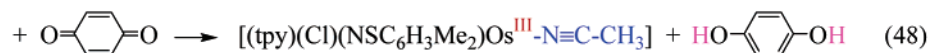
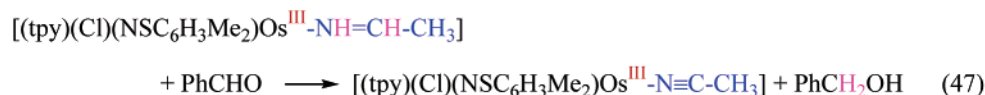
Wave II



Wave III



## Scheme 23



Addition of water causes a dramatic change in the cyclic voltammogram. New waves labeled II and III in Figure 13 appear, and both are pH-dependent. The  $E_{1/2}$  values for II decrease by 57 mV/pH unit over an extended pH range. It is a two-electron wave as shown by peak current comparisons and coulometry. Electrochemical reduction past this wave results in reduction of coordinated acetonitrile ( $\text{N}\equiv\text{C}-\text{CH}_3$ ) to coordinated imine ( $\text{NH}=\text{CH}-\text{CH}_3$ ), eq 45 (Scheme 22).

The  $\text{Os}^{\text{III}}-\text{NH}=\text{CH}-\text{CH}_3$  product has been characterized spectroscopically by  $^1\text{H}$  NMR and IR measurements. Although there is an extensive published redox chemistry based on  $\text{CH}_3\text{CN}$ , this is the first example of a simple reversible  $2\text{e}^-/2\text{H}^+$  couple. As shown by the electrochemical measurements, it is kinetically facile and appears to be another example of activation by electronic coupling with Os. The second, irreversible wave labeled III is a multielectron wave. Reduction past this wave results in further reduction of the imine by two electrons and two protons to give ethylamine, eq 46 (Scheme 22), as shown by GC-MS.

The facile interconversion between imino and nitrile shown by the electrochemical results suggests that the bound ligand-based couple may also be a useful reagent for reduction or

oxidation of other substrates. We have explored this possibility by investigating the reactions of the  $\text{Os}(\text{III})$ -imino complex with three reagents, i.e., benzaldehyde (eq 47), quinone (eq 48), and di(2-pyridyl)ketone (eq 49) (Scheme 23).

The reactions with benzaldehyde, quinone, and di(2-pyridyl)ketone are first order in Os and first order in substrate and occur with  $k_{\text{PhCHO}}(25.0 \pm 0.1 \text{ }^\circ\text{C}) = (1.03 \pm 0.01) \times 10^{-2} \text{ M}^{-1} \text{ s}^{-1}$ ,  $k_{\text{quinone}}(25.0 \pm 0.1 \text{ }^\circ\text{C}) = (3.63 \pm 0.01) \times 10^2 \text{ M}^{-1} \text{ s}^{-1}$ , and  $k_{\text{py}_2\text{CO}}(25.0 \pm 0.1 \text{ }^\circ\text{C}) = (1.07 \pm 0.01) \times 10^{-2} \text{ M}^{-1} \text{ s}^{-1}$ . The organic products were extracted from 3:1 (v/v)  $\text{CH}_3\text{CN}:\text{H}_2\text{O}$  mixtures with hexane and identified by GC-MS. The ligand-based redox chemistry may be useful for the reduction or oxidation of organic compounds, perhaps catalytically. The mechanistic details remain to be elucidated.

**Acknowledgment** is made for support of this research to the National Science Foundation, the National Institutes of Health, and the Los Alamos National Laboratory.

IC020731V